Long-range ferroelectric order in two-dimensional excitonic insulators

M. M. Glazov [1,*] and A. İmamoğlu [2,†]
[1] *Ioffe Institute, St. Petersburg 194021, Russia*
[2] *Institute for Quantum Electronics, ETH Zürich, CH-8093 Zürich, Switzerland*

(Received 14 December 2025; accepted 23 July 2026; published 24 August 2026)

It is generally argued that Mermin-Wagner theorem excludes the possibility of long-range order in two-dimensional bosonic systems at nonzero temperatures. In contrast, we show here that generic bilayer semiconductors could demonstrate true Bose-Einstein condensation of interlayer excitons. We find that the key requirements include (1) reduction of the interlayer band gap using an applied electric field so that excitons spontaneously appear in the ground state, (2) band structure that allows for long-range electron-hole exchange interaction, and (3) a finite magnetic field. When these conditions are fulfilled, superfluidity and ferroelectric order can coexist in two-dimensional excitonic insulators. Our results provide an example where coupling to the vacuum electromagnetic near field leads to a finite temperature second-order phase transition.

DOI: 10.1103/mvym-8n1z

I. INTRODUCTION AND MOTIVATION

Interlayer excitons in transition metal dichalcogenide (TMD) bilayers constitute a promising platform for observation of the elusive excitonic insulator state [1–8]. By applying a finite electric field [Fig. 1(a)], it is possible to reduce the interlayer band gap E_g, defined as the energy difference between the conduction band minimum of one layer and the valence band maximum of the other layer, so that it is smaller than the binding energy of the interlayer $1s$ exciton (E_B): In this limit, interlayer excitons appear spontaneously in the ground state [9]. However, Mermin-Wagner theorem excludes the possibility for continuous symmetry breaking at finite temperature T for two-dimensional (2D) systems with short-range hopping or interactions [10,11]. Because the center-of-mass motion of interlayer excitons generically has a parabolic dispersion that is linked to short-range hopping, it is widely assumed that a $T > 0$ excitonic insulator state with true long-range order is not possible even in the limit $E_B > E_g$.

On the other hand, it is well known that coupling of optically active 2D intralayer excitons to the three-dimensional electromagnetic field vacuum substantially modifies their excitation spectra: Within the light cone, light-matter coupling leads to a finite spontaneous emission rate. Outside the light cone, the strong interaction with electromagnetic near field results in a splitting of the excitonic bands: While excitons that are polarized transversally (T) to the center-of-mass momentum k exhibit parabolic dispersion, longitudinally polarized (L) excitons acquire linear dispersion [12–15]. The origin of linear dispersion can be traced back to flip-flop dipole-dipole interaction that leads to long-range hopping, scaling as $1/r^3$ [16,17]. However, since the contribution of light-matter coupling to exciton self-energy is purely imaginary for $k \to 0$, finite-energy intralayer excitons at $E_x(k = 0) = E_x = E_g - E_B > 0$ cannot exhibit continuous symmetry breaking, even though a laserlike nonequilibrium transition to a coherent state with weak phase diffusion cannot be ruled out.

In this work, we show that for ground-state interlayer excitons under external magnetic field, the exciton dispersion in the limit $k \to 0$ is linear, provided that $k \neq 0$ excitons have in-plane dipolar coupling to the electromagnetic field. After carrying out a mean-field analysis using a Bardeen-Cooper-Schrieffer (BCS) variational ansatz to show the formation of a condensate for $T = 0$ without any external phase fixing, we analyze the spectrum of excitations and derive how coupling to the electromagnetic field modifies the dispersion of the elementary Bogoluibov excitations. Finally, we show that the thermally excited exciton density remains finite for $T > 0$, signaling the emergence of a true long-range order at a critical temperature $T_c > 0$.

Our analysis assumes that the interlayer excitons in the limit $E_g > E_B$ occupy a single valley and couple either to right- or left-hand circularly polarized fields within the light cone. When $E_B > E_g$ and $T > T_c$, the excitons do not have a well-defined in-plane polarization but a finite small static polarization along the direction z that separates the two layers. Upon condensation, the ground-state excitons acquire a large in-plane polarization, realizing a ferroelectric phase transition that is not linked to a structural phase transition [18–20]. We emphasize that the emergence of an ordered ferroelectric phase upon spontaneous breaking of U(1) symmetry associated with in-plane exciton polarization constitutes an example where vacuum fluctuations qualitatively modify the ground state of an electronic system.

*Contact author: glazov@coherent.ioffe.ru
†Contact author: imamoglu@phys.ethz.ch

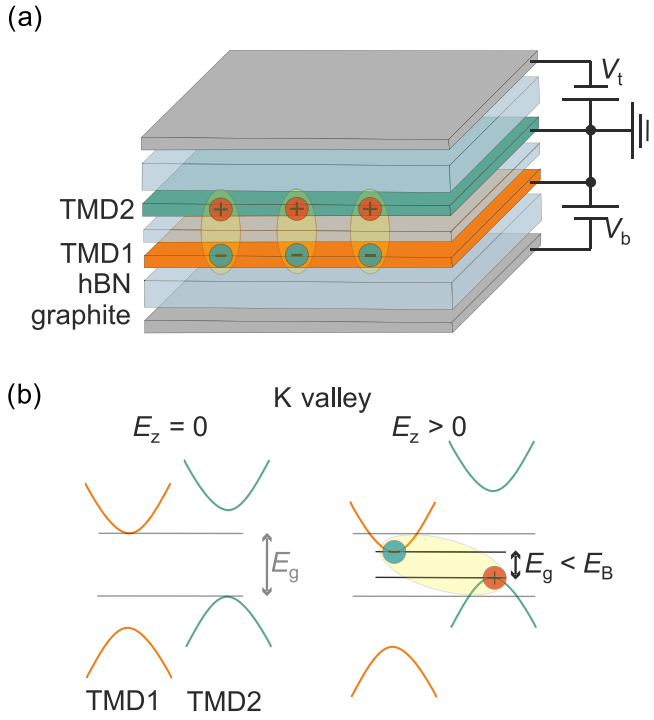

FIG. 1. (a) The van der Waals heterostructure that we analyze. The two TMD layers have type II band alignment and they are either in direct contact or are separated by monolayer hexagonal boron nitride (hBN). Voltages applied on top and bottom graphite gates are used to adjust the vertical electric field E_z. (b) Sketch of the band diagram around the K valley. The spatially indirect band gap E_g can be tuned via electric field E_z to reach $E_g < E_B$ to ensure that interlayer excitons appear spontaneously.

II. DERIVATION OF THE EXCITON GAP EQUATION

Here, we show the steps leading to the exciton gap equation, identifying the linear and nonlinear contributions arising from electron-hole attraction, as well as the effects of the electron-electron and hole-hole interactions and phase space filling. We then show that the gap equation admits a nontrivial solution indicating excitonic instability if the band gap is smaller than the exciton binding energy.

What distinguishes our analysis from the majority of prior work is the inclusion of interlayer coupling [8]: For direct tunnel coupling between the conduction and valence bands, we obtain a source term for the order parameter that fixes the phase and amplitude; the resulting gap equation is reminiscent of resonant laser excitation of excitons. Remarkably, when the interband coupling is of chiral p-wave form, that is, it is proportional to $k_x \pm ik_y$, no phase fixing occurs. As we further show, interlayer coupling of this form, together with (i) exciton binding energy larger than the bare band gap and (ii) application of the magnetic B field, leads to linear dispersion of excitons as $k \to 0$, which in turn ensures the existence of true long-range order.

A. Hamiltonian of the bilayer system

We consider a heterobilayer structure with type-II band alignment depicted in Fig. 1. Let layer 1 be the "electron" layer and layer 2 be the "hole" layer; i.e., the conduction band minimum of the bilayer corresponds to the layer 1 (band $c1$) and the valence band minimum to the layer 2 (band $v2$). We disregard the spin and valley degrees of freedom considering the bottom conduction band and top valence band in one of the valleys K_+ or K_-. This assumption is justified since the spin-orbit splitting of the conduction and valence bands at $K_\pm$ points amounts to $\sim$10 and $\sim$100 meV, respectively.

We are interested in the long-range coherence, i.e., in the long-wavelength or small wave-vector properties of excitons. Hence, we start from the 2×2 effective Hamiltonian describing the nearest conduction and valence band states (see Appendix A for derivation):

$$\mathcal{H}_2 = \begin{pmatrix} E_c(\boldsymbol{k}) & \gamma_\alpha k_\alpha \\ \gamma_\alpha^* k_\alpha & E_v(\boldsymbol{k}) \end{pmatrix}, \tag{1}$$

where

$$E_c(\boldsymbol{k}) = \frac{E_g}{2} + \frac{\hbar^2 k^2}{2m_e}, \tag{2a}$$

$$E_v(\boldsymbol{k}) = -\frac{E_g}{2} - \frac{\hbar^2 k^2}{2m_h}. \tag{2b}$$

Here, $m_e, m_h > 0$ are the effective masses of the electrons and holes in the absence of interlayer coupling, E_g is the effective band gap, and γ_α ($\alpha = x, y$) are the effective interband momentum matrix elements. To proceed, we assume that γ_α are much smaller than the other relevant energy scales and the dispersion of the charge carriers is mainly controlled by the diagonal terms in the Hamiltonian provided that $E_g \gg |\gamma_\alpha k_\alpha|$.

We rewrite the Hamiltonian (1) in the second quantization representation, introducing the conduction band creation (annihilation) operators $\hat{a}_{\boldsymbol{k}}^\dagger$ ($\hat{a}_{\boldsymbol{k}}$) and the valence band hole creation (annihilation) operators $\hat{b}_{\boldsymbol{k}}^\dagger = \hat{a}_{v,-\boldsymbol{k}}$ ($b_{\boldsymbol{k}} = \hat{a}_{v,-\boldsymbol{k}}^\dagger$). Equation (1) reads

$$\mathcal{H}_2 = \sum_{\boldsymbol{k}} E_c(\boldsymbol{k}) \hat{a}_{\boldsymbol{k}}^\dagger \hat{a}_{\boldsymbol{k}} + \sum_{\boldsymbol{k}} E_h(\boldsymbol{k}) \hat{b}_{\boldsymbol{k}}^\dagger \hat{b}_{\boldsymbol{k}} + \sum_{\boldsymbol{k}} \left(\Lambda_{\boldsymbol{k}} \hat{a}_{\boldsymbol{k}}^\dagger \hat{b}_{-\boldsymbol{k}}^\dagger + \text{H.c.} \right), \tag{3}$$

where we introduced the hole dispersion $E_h(\boldsymbol{k}) = -E_v(-\boldsymbol{k})$ and interband coupling $\Lambda_{\boldsymbol{k}} = \gamma_\alpha k_\alpha$. The coupling has a chiral p-wave form related to the different symmetries of the conduction and valence bands and allowed optical transition between the bands. Here, we assume that the two layers are R stacked (0°) with a fixed displacement that ensures C_3 symmetry and circularly polarized interlayer dipole coupling in K_+ or K_- valleys. The symmetry analysis shows that the chiral selection rules for optical transitions in high-symmetry heterobilayer stacking remain [21–23]. Hence, relatively weak spin-orbit mixing of the bands does not change the form of interband coupling $\Lambda_{\boldsymbol{k}}$ in Eq. (3). If direct interband tunneling were possible, $\Lambda_{\boldsymbol{k}}$ would contain a wave-vector-independent contribution.

Excitons form because of the Coulomb attraction between electrons and holes. Let $V_{\boldsymbol{q}} > 0$ be the Fourier transform of the Coulomb interaction potential within the same layer and let d be the interlayer distance. Hence, the electron-electron,

hole-hole, and electron-hole contributions read

$$\mathcal{V} = \frac{1}{2}\sum_{\boldsymbol{k},\boldsymbol{k}',\boldsymbol{q}} V_{\boldsymbol{q}}\big(\hat{a}^\dagger_{\boldsymbol{k}}\hat{a}^\dagger_{\boldsymbol{k}'}\hat{a}_{\boldsymbol{k}'+\boldsymbol{q}}\hat{a}_{\boldsymbol{k}-\boldsymbol{q}} + \hat{b}^\dagger_{\boldsymbol{k}}\hat{b}^\dagger_{\boldsymbol{k}'}\hat{b}_{\boldsymbol{k}'+\boldsymbol{q}}\hat{b}_{\boldsymbol{k}-\boldsymbol{q}} - 2e^{-qd}\hat{a}^\dagger_{\boldsymbol{k}}\hat{b}^\dagger_{\boldsymbol{k}'}\hat{b}_{\boldsymbol{k}'+\boldsymbol{q}}\hat{a}_{\boldsymbol{k}-\boldsymbol{q}}\big). \tag{4}$$

The prefactor e^{-qd} takes into account slight reduction of the interlayer interaction as compared to the intralayer one; see Ref. [24] for more advanced models. Equation (4) takes into account the static Coulomb interaction that is responsible for formation of the excitons. We will analyze the long-range exchange interaction related to the macroscopic electromagnetic fields produced by the excitons in Sec. III using an electrodynamical approach.

B. Gap equation and order parameter

We now analyze the possibility of exciton insulator formation. It is convenient to assume the BCS form of the many-body wavefunction

$$\Psi = \prod_{\boldsymbol{k}} \big(u_{\boldsymbol{k}} + v_{\boldsymbol{k}} a^\dagger_{\boldsymbol{k}} b^\dagger_{-\boldsymbol{k}}\big)|0\rangle, \tag{5}$$

where $|0\rangle$ is the ground state of the system with the filled valence band and the empty conduction band and $u_{\boldsymbol{k}}$, $v_{\boldsymbol{k}}$ are the coefficients that together quantify electron-hole pairing. We consider the $T = 0$ case and study the pairing in the lowest-energy state corresponding to zero net momentum of excitons. Neglecting for simplicity the electron-electron and hole-hole repulsion and making standard transformations [1,2,25–33], we obtain the exciton gap $\Delta_{\boldsymbol{k}} = \sum_{\boldsymbol{k}'} V_{\boldsymbol{k}-\boldsymbol{k}'} u^*_{\boldsymbol{k}'} v_{\boldsymbol{k}'}$ equation in the form

$$\Delta_{\boldsymbol{k}} = \sum_{\boldsymbol{k}'} V_{\boldsymbol{k}-\boldsymbol{k}'} \frac{\Delta_{\boldsymbol{k}'}}{\mathcal{E}_{\boldsymbol{k}'}} + \Lambda_{\boldsymbol{k}}, \tag{6}$$

where the renormalized energy reads

$$\mathcal{E}_{\boldsymbol{k}} = \sqrt{[E_e(\boldsymbol{k}) + E_h(-\boldsymbol{k})]^2 + 4\Delta^2_{\boldsymbol{k}}}. \tag{7}$$

We analyze the effect of finite T in Appendix B.

For low condensate density, $\Delta_{\boldsymbol{k}} \to 0$, Eq. (6) can be recast in somewhat different form convenient for the following analysis. To that end, we decomposne $\mathcal{E}_{\boldsymbol{k}}$ into series in $\Delta_{\boldsymbol{k}}$ keeping only the zero- and second-order terms and introduce the wavefunction $\Psi_{\boldsymbol{k}} = u^*_{\boldsymbol{k}} v_{\boldsymbol{k}} = \Delta_{\boldsymbol{k}}/\mathcal{E}_{\boldsymbol{k}} \approx \Delta_{\boldsymbol{k}}/[E_e(\boldsymbol{k}) + E_h(-\boldsymbol{k})]$ that, upon expanding $\Delta_{\boldsymbol{k}}/\mathcal{E}_{\boldsymbol{k}}$ to lowest order, gives

$$[E_e(\boldsymbol{k}) + E_h(-\boldsymbol{k})]\Psi_{\boldsymbol{k}} - \sum_{\boldsymbol{k}} V_{\boldsymbol{k}-\boldsymbol{k}'}\Psi_{\boldsymbol{k}'} + 2\sum_{\boldsymbol{k}'} V_{\boldsymbol{k}-\boldsymbol{k}'}|\Psi_{\boldsymbol{k}'}|^2\Psi_{\boldsymbol{k}'} = \Lambda_{\boldsymbol{k}}. \tag{8}$$

We note that inclusion of the repulsion between the charge carriers of the same polarity modifies the nonlinear term in Eq. (8) (see Ref. [28] and Appendix C).

The nonlinear gap equation [Eq. (6) or Eq. (8)] admits, in general, different types of solutions. The first type corresponds to solutions of inhomogeneous equations (6) and (8) that vanish as $\Lambda_{\boldsymbol{k}} \to 0$. These induced or forced solutions are somewhat trivial, since they correspond to the presence of interband correlations as a result of the coupling described by the term $\propto \Lambda_{\boldsymbol{k}}$ in the Hamiltonian (3). Importantly, there is a second class of solutions of the gap equation that are nonzero as $\Lambda_{\boldsymbol{k}} \to 0$. These solutions of the second type, which describe spontaneous pairing in the system, are what we focus on.

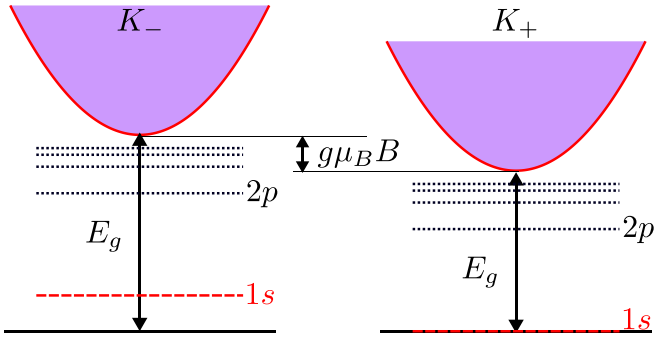

FIG. 2. Schematic illustration of the heterobilayer excitonic band structure in the presence of magnetic field induced Zeeman splitting $g\mu_B B$, where g is the exciton g factor, μ_B is the Bohr magneton, and B is the normal component of the magnetic field. Series of bound excitonic states are shown by the dashed ($1s$ state) and dotted ($2p$ and other higher-lying states) lines. Parabolas show the continuum states of electron-hole pairs. It is seen that the exciton insulator instability condition (9) is first met for $1s$ exciton in the K_+ valley.

We first set $\Lambda_{\boldsymbol{k}} = 0$ and analyze the instabilities in the system. In the vicinity of the pairing onset, $\Psi_{\boldsymbol{k}}$ in Eq. (8) is vanishingly small and the nonlinear term becomes negligible. Thus, Eq. (8) reduces to the Schrödinger equation describing the Coulomb attraction of the electron and the hole, which has nontrivial solutions provided that the Coulomb interaction is sufficiently large to ensure that the lowest energy bound eigenstate has zero energy; i.e., the binding energy of this state is equal to the band gap E_g. Naturally, when reducing E_g using the applied electric field, the first state to reach zero energy is the ground, $1s$ exciton state (Fig. 2). Hence, under the condition

$$E_B \geqslant E_g, \tag{9}$$

where E_B is the $1s$ exciton binding energy, excitons form spontaneously in the ground state. The wavefunction can be written as

$$\Psi_{\boldsymbol{k}} = a\varphi^{1s}_{\boldsymbol{k}} = |a|e^{i\chi}\varphi^{1s}_{\boldsymbol{k}}, \tag{10}$$

where $\varphi^{1s}_{\boldsymbol{k}}$ is the normalized $1s$ exciton wavefunction in momentum space and a is the complex parameter with its absolute value $|a|$ and phase χ. The amplitude a of the exciton condensate can be found from Eq. (8) by substituting $\Psi_{\boldsymbol{k}}$ in the form of Eq. (10), multiplying by $\varphi^{1s*}_{\boldsymbol{k}}$ and summing over $\boldsymbol{k}$:

$$(E_g - E_B)a = -g|a|^2 a + \lambda, \tag{11}$$

where we restored the inhomogeneous term,

$$\lambda = \sum_{\boldsymbol{k}} \varphi^{1s*}_{\boldsymbol{k}} \Lambda_{\boldsymbol{k}}. \tag{12}$$

Equation (11) contains the effective nonlinear "interaction" term with the interaction parameter

$$g = \sum_{\boldsymbol{k}} |\varphi_{\boldsymbol{k}}^{1s}|^4 \left(E_B + \frac{\hbar^2 k^2}{2\mu} \right) > 0. \tag{13}$$

The electron-electron and hole-hole repulsion contributions that we neglected change the expression for g but do not significantly alter the analysis and conclusions of this work (see Appendix C for details). Equation (11) corresponds to the equation for the order parameter in the generic ϕ^4 theory of continuous phase transitions.

In the experimentally relevant case of TMD heterobilayers, the conduction and valence bands have different symmetry [21,22] and the interband coupling terms $\Lambda_{\boldsymbol{k}}$ are proportional to the combinations of the wave-vector components k_α [see Eqs. (3) and (A2c)] [8]. This is typical for semiconductor systems with dipole-allowed interband optical transition: The interband momentum matrix element γ_α [Eq. (3)] is nonzero between the Bloch functions whose angular momentum component is different by 1. Since the $1s$ exciton wavefunction is axially symmetric, $\lambda \equiv 0$. Equation (11) is therefore homogeneous and the phase of a is arbitrary despite the presence of interband coupling. This is the distinguishing feature of the system we analyze in comparison to the previously investigated models where the bands were essentially of the same symmetry, leading to $\lambda \neq 0$, and the condensate phase was fixed by the interband coupling, see Refs. [28–31]; the latter case is similar to the case where a coherent state of excitons is generated by a resonant laser field.

Hence, in contrast to the common knowledge [28,31], in two-dimensional semiconductors with different symmetries of conduction and valence bands the exciton condensation upon varying E_g is a second-order quantum phase transition: The phase of the condensate is arbitrary. Note that for the $\boldsymbol{k}$-linear interband coupling the phase could be fixed for p excitons with odd envelope functions. However, their binding energies are significantly smaller than for $1s$ state. Hence, an instability in the system occurs first for the $1s$ exciton, where the phase is arbitrary. These results also follow from more general equation (6).

The solution of Eq. (11) in the relevant case of $\lambda = 0$ is simple:

$$a = \begin{cases} 0, & E_g > E_B, \\ e^{i\chi} g^{-1/2} \sqrt{E_B - E_g}, & E_g < E_B, \end{cases} \tag{14}$$

where χ is an arbitrary phase. Naturally, as soon as condition (9) is met, the order parameter spontaneously appears in the system. In accordance with Eq. (5), the many-body wavefunction of the system can be represented as a coherent state:

$$\Psi \propto |0\rangle + a|1\rangle + \frac{a^2}{\sqrt{2!}}|2\rangle + \frac{a^3}{\sqrt{3!}}|3\rangle \cdots, \tag{15}$$

where $|1\rangle = \sum_{\boldsymbol{k}} \varphi_{\boldsymbol{k}}^{1s} a_{\boldsymbol{k}}^\dagger b_{-\boldsymbol{k}}^\dagger |0\rangle$ is the state with a single exciton in the system; states with higher exciton number ($|2\rangle$, $|3\rangle$) can be expressed similarly.

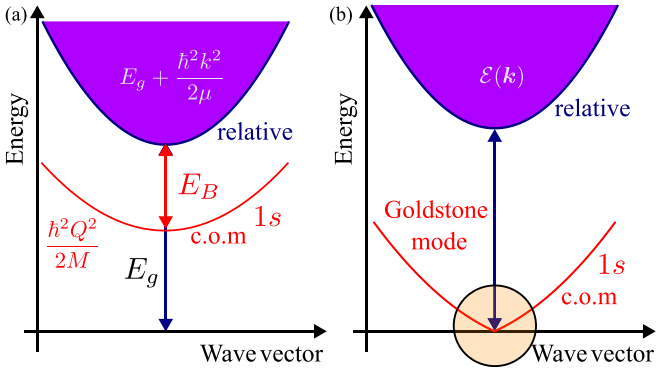

FIG. 3. Spectrum of excitations. Only one bound state, $1s$, is shown. (a) Noncondensed system, $\Delta = 0$. The excitations correspond to the exciton center-of-mass motion with parabolic dispersion (red parabola) and relative motion of electron-hole pairs in continuum (shaded region bounded by blue parabola). Here, we neglect the weak light-matter interaction. (b) Excitonic insulator state, $\Delta = 0$. The relative motion continuum (shaded region bounded by blue parabola) is separated by the gap $\sqrt{E_g^2 + 4\Delta^2}$ from the condensate ground state. Red curve sketches the dispersion of the collective, Goldstone mode. Orange region of small momenta is of interest for analysis of the condensate stability.

So far, we have analyzed the $T = 0$ limit. We now focus on the case where $E_B \geqslant E_g$ and consider the T dependence of ground-state excitons. The high-temperature scale of our problem is the pairing temperature T_{pair} below which a thermal state of excitons appears: We estimate T_{pair} in Appendix B. Superfluidity without long-range order emerges for $T < T_{\text{BKT}}$, where T_{BKT} is the Berezinskii-Kosterlitz-Thouless transition temperature [34–36]. The critical temperature T_c for condensation is even lower and is linked to the suppression of phase fluctuations of the order parameter (see Sec. IV) . Since excitons are charge neutral, the lowest-energy collective excitations correspond to the gapless Goldstone mode [Fig. 3(b)]. To analyze the stability of the exciton condensate, we need to determine the spectrum of collective excitations, which, as shown below, are strongly affected by the coupling to the electromagnetic field.

III. LIGHT-MATTER INTERACTION

In this section, we analyze the response of the excitonic insulator to the electromagnetic field vacuum. We focus on the case where an external magnetic field ensures that the lowest-energy interlayer exciton state is the $1s$ exciton in K_+ valley due to valley Zeeman effect (Fig. 2). We also assume that the intervalley states where the electron and hole occupy different valleys have higher energy. In this regime, the pairing threshold (9) is reached in the K_+ valley where $\Lambda_{\boldsymbol{k}} \propto k_x - ik_y$. To describe the light-matter interaction, we introduce the matrix element of the in-plane dipole moment of the interband exciton $\hat{\boldsymbol{d}}$:

$$\langle \text{exc}|\hat{\boldsymbol{d}}|0\rangle = \frac{d_{\text{exc}}}{\sqrt{2}}(\hat{\boldsymbol{x}} - i\hat{\boldsymbol{y}}), \tag{16}$$

where $\hat{\boldsymbol{x}}, \hat{\boldsymbol{y}}$ are the unit vectors along the respective coordinate axes and $d_{\text{exc}} \propto |\lambda_\alpha| \varphi_{1s}(\mathbf{r} = 0)$ is a real parameter. For the

exciton in the K_- valley, the sign on the right-hand side of Eq. (16) should be reversed. The exciton insulator described by the coherent state (15) is characterized by a nonzero static dipole moment $\boldsymbol{P}$ with the in-plane components

$$P_x = \frac{d_{\rm exc}}{\sqrt{2}}(a + a^*), \quad P_y = \frac{d_{\rm exc}}{\sqrt{2}}{\rm i}(a - a^*). \tag{17}$$

Hence, the polarization arises as a linear function of the condensate order parameter a and its orientation in the heterostructure plane is determined by the phase χ. Consequently, fixing of χ upon transition to the exciton insulator state can be viewed as a transition to a ferroelectric state with finite in-plane polarization (cf. Refs. [18,19]). We remark that, because of the heterobilayer asymmetry, there is also a z component of the static dipole moment

$$P_z = d_z|a|^2, \tag{18}$$

which is quadratic in order parameter and controlled by the static z component of the exciton dipole. In what follows, we assume the limit of small $|a|$ and ignore $P_z \propto |a|^2$ in comparison to $P_x, P_y \propto a$; we leave the analysis of the more general case where P_z is non-negligible to future work. We also stress that in the systems where the conduction and valence bands possess the same symmetry and $d_{\rm exc} \equiv 0$, not only the phase of the exciton condensate becomes fixed (see Sec. II B) but also the spontaneous in-plane ferroelectric polarization in Eq. (17) is absent.

It is straightforward to extend Eq. (11) to allow for smooth spatial and temporal dynamics of the order parameter. Taking into account the center-of-mass coordinate $\boldsymbol{R}$ of the excitons, we obtain

$$\begin{aligned} {\rm i}\hbar\frac{\partial a(\boldsymbol{R},t)}{\partial t} &= -\frac{\hbar^2}{2M}\Delta_{\boldsymbol{R}} a(\boldsymbol{R},t) + (E_g - E_B)a(\boldsymbol{R},t) \\ &\quad + g|a(\boldsymbol{R},t)|^2 a(\boldsymbol{R},t) - d_{\rm exc}E^{\sigma^+}(\boldsymbol{R},t), \end{aligned} \tag{19}$$

where $M = m_e + m_h$ is the exciton mass describing the center-of-mass motion and $\boldsymbol{E}(\boldsymbol{R},t)$ is the electric field vector:

$$\boldsymbol{E}(\boldsymbol{R},t) = \boldsymbol{E}_{\boldsymbol{Q},\Omega} e^{{\rm i}\boldsymbol{Q}\boldsymbol{R} - {\rm i}\Omega t} + \boldsymbol{E}_{-\boldsymbol{Q},-\boldsymbol{\Omega}} e^{-{\rm i}\boldsymbol{Q}\boldsymbol{R} + {\rm i}\Omega t}, \tag{20}$$

where $\boldsymbol{E}_{-\boldsymbol{Q},-\boldsymbol{\Omega}} = \boldsymbol{E}^*_{\boldsymbol{Q},\boldsymbol{\Omega}}$,

$$E^{\sigma^\pm}_{\boldsymbol{Q},\Omega} = \frac{E_{x;\boldsymbol{Q},\Omega} \mp {\rm i}E_{y;\boldsymbol{Q},\Omega}}{\sqrt{2}}, \tag{21}$$

are the corresponding circularly polarized components. Equation (19) is similar to the Gross-Pitaevskii equation for the wavefunction of the condensate of weakly interacting bosons [37]. Naturally, $|a|^2$ is the condensate density, the quantity $\phi_{\rm chem} = E_B - E_g$ plays a role of the chemical potential, and the parameter g plays a role of the interaction constant. The relation $\phi_{\rm chem} = g|a|^2$ follows directly from Eq. (14). The term $-d_{\rm exc}E^{\sigma^+}$ describes the coupling of the dipole-active exciton condensate with the electric field of electromagnetic wave.

Presenting $a(\boldsymbol{R},t)$ in the form

$$a(\boldsymbol{R},t) = ae^{{\rm i}\chi} + fe^{{\rm i}\boldsymbol{Q}\boldsymbol{R} - {\rm i}\Omega t} + w^* e^{2{\rm i}\chi - {\rm i}\boldsymbol{Q}\boldsymbol{R} + {\rm i}\Omega t}, \tag{22}$$

where a satisfies Eq. (14), $\boldsymbol{Q}$ is the wave vector of the excitation, and Ω is its frequency, we obtain the set of equations for the amplitudes f and w:

$$\hbar\Omega f = \frac{\hbar^2 Q^2}{2M} f + (E_B - E_g)(f + w) - d_{\rm exc}E^{\sigma^+}_{\boldsymbol{Q},\Omega}, \tag{23}$$

$$\begin{aligned} -\hbar\Omega w &= \frac{\hbar^2 Q^2}{2M} w + (E_B - E_g)(f + w) \\ &\quad - d^*_{\rm exc}e^{2{\rm i}\chi}E^{\sigma^-}_{\boldsymbol{Q},\Omega}. \end{aligned} \tag{24}$$

To determine the spectrum of elementary excitations in the absence of light-matter interaction, we set $\boldsymbol{E}(\boldsymbol{R},t) = 0$ and arrive at the standard dispersion of the condensate excitations in the form

$$\varepsilon(\boldsymbol{Q}) = \sqrt{\left(\frac{\hbar^2 Q^2}{2M}\right)^2 + \frac{\hbar^2 Q^2}{M}(E_B - E_g)}. \tag{25}$$

In particular, for $Q \to 0$ the spectrum is soundlike, as one expects for weakly interacting bosons [37]:

$$\varepsilon(Q) = \hbar c_s Q, \quad c_s = \sqrt{\frac{E_B - E_g}{M}}, \tag{26}$$

where c_s is the effective Bogoliubov velocity (speed of sound in the condensate); the difference $E_B - E_g > 0$ is the chemical potential of the condensate (see above). We recall that in two-dimensional systems such form of excitation spectrum prevents true condensation at finite T [see Eq. (43) below]. In the next section, we show that the allowance for the coupling of excitons with the vacuum electromagnetic field drastically changes the situation and allows for the true Bose-Einstein condensation.

We now calculate the response of the exciton insulator with respect to the external electromagnetic field. Let us select the in-plane coordinate system in such a way that x axis is aligned with the static polarization $\boldsymbol{P}$, which is equivalent to setting $\chi = 0$. Introducing two response functions ($E_B \geqslant E_g$)

$$\pi_1(\Omega,\boldsymbol{Q}) = d^2_{\rm exc}\frac{E_B - E_g + \frac{\hbar^2 Q^2}{2M} + \hbar\Omega}{\varepsilon^2(\boldsymbol{Q}) - (\hbar\Omega)^2}, \tag{27a}$$

$$\pi_2(\Omega,\boldsymbol{Q}) = d^2_{\rm exc}\frac{E_B - E_g}{\varepsilon^2(\boldsymbol{Q}) - (\hbar\Omega)^2}, \tag{27b}$$

we have

$$P^{\sigma^+}_{\boldsymbol{Q},\Omega} = \pi_1(\Omega,\boldsymbol{Q})E^{\sigma^+}_{\boldsymbol{Q},\Omega} - \pi_2(\Omega,\boldsymbol{Q})E^{\sigma^-}_{\boldsymbol{Q},\Omega}, \tag{28a}$$

$$P^{\sigma^-}_{\boldsymbol{Q},\Omega} = \pi_1(-\Omega,\boldsymbol{Q})E^{\sigma^-}_{\boldsymbol{Q},\Omega} - \pi_2(\Omega,\boldsymbol{Q})E^{\sigma^+}_{\boldsymbol{Q},\Omega}, \tag{28b}$$

where we took into account that oscillatory components of polarization are related to the coefficients f and w in Eq. (22) as $P^{\sigma^+}_{\boldsymbol{Q},\Omega} = d_{\rm exc}f$, and $P^{\sigma^-}_{\boldsymbol{Q},\Omega} = d_{\rm exc}w$. For completeness, we note that in the absence of condensate $\pi_2(\Omega,\boldsymbol{Q}) \equiv 0$, while $\pi_1(\Omega,\boldsymbol{Q})$ reduces to

$$\pi_1(\Omega,\boldsymbol{Q}) = \frac{d^2_{\rm exc}}{E_g - E_B + \frac{\hbar^2 Q^2}{2M} - \hbar\Omega}. \tag{29}$$

Interestingly, the optical response of the system described by Eq. (28) is anisotropic in the presence of the exciton condensate. Indeed, the right-hand circularly polarized component of oscillatory polarization can be induced not only by

the component of the incident electromagnetic fields with the same helicity, but also by the left-hand circularly polarized fields (and vice versa). This polarization conversion effect is described by the response function $\pi_2(\Omega, \boldsymbol{\Omega})$ that vanishes in the absence of the condensate. Physically, $\pi_2(\Omega, \boldsymbol{\Omega})$ emerges due to the optical anisotropy of the system in the presence of the order parameter $a \neq 0$. This condensate-induced anisotropy of the system is also clearly seen in the linearly polarized basis; it is particularly strong in the small $\boldsymbol{Q}$, Ω regime where

$$\hbar\Omega,\ \varepsilon(\boldsymbol{Q}),\ \frac{\hbar^2 Q^2}{2M} \ll E_B - E_g. \tag{30}$$

Equation (30) corresponds to the range of wave vectors and frequencies where the condensate effects are dominant. Here, $\pi_1(\Omega, \boldsymbol{Q}) \approx \pi_2(\Omega, \boldsymbol{Q})$ and, hence,

$$P_{x;\boldsymbol{Q},\Omega} \approx -\mathrm{i}d_{\mathrm{exc}}^2 E_{y;\boldsymbol{Q},\Omega} \frac{\hbar\Omega}{\varepsilon^2(\boldsymbol{Q}) - (\hbar\Omega)^2}, \tag{31a}$$

$$\begin{aligned} P_{y;\boldsymbol{Q},\Omega} &= 2\pi_1(\Omega, \boldsymbol{Q}) E_{y;\boldsymbol{Q},\Omega} \\ &\approx 2d_{\mathrm{exc}}^2 E_{y;\boldsymbol{Q},\Omega} \frac{E_B - E_g}{\varepsilon^2(\boldsymbol{Q}) - (\hbar\Omega)^2}. \end{aligned} \tag{31b}$$

We recall that we use the frame of axes where the static polarization of the condensate $\boldsymbol{P} \parallel x$. Here, the response along the x axis is strongly suppressed, while the response along the y axis is prominent. At fixed E_y, we have $|P_x/P_y| \sim \hbar\Omega/(E_B - E_g) \ll 1$. Electric fields polarized along the x axis tend to change the amplitude of the order parameter, and such changes are energetically costly, while the field polarized along the y axis tends to rotate the order parameter while preserving its magnitude; this rotation corresponds to variation of the overall condensate phase.

IV. PHASE FLUCTUATIONS AND TRUE CONDENSATION

The long-wavelength low-frequency Goldstone mode associated with the phase fluctuations of the order parameter [Eq. (25)] plays a crucial role in the response and stability of condensates. In particular, thermal fluctuations of the order parameter phase are known to destroy the long-range order in two-dimensional systems with broken continuous symmetries [10,11], resulting in Berezinskii-Kosterlitz-Thouless physics for small but nonzero T [34–36]. Here, we study phase fluctuations in the exciton insulator phase and demonstrate that for optically active excitons the coupling with the electromagnetic field suppresses the effect of thermal fluctuations and stabilizes a true Bose-Einstein condensate for $T > 0$.

We start with the analysis of the spectrum of elementary excitation of excitonic insulator by taking into account light-matter interaction. To this end, we complement the material relation in the form of Eq. (31) by the solution of Maxwell's equations that relates the electric field with the polarization produced by the excitations of the condensate:

$$E_{\alpha,\Omega} = \sum_{\beta} D^E_{\alpha\beta}(\Omega, \boldsymbol{Q}) P_{\beta;\boldsymbol{Q},\Omega}, \tag{32a}$$

where the electromagnetic Green's function takes the form [38]

$$D^E_{\alpha\beta}(\Omega, \boldsymbol{Q}) = \frac{2\pi(\Omega/c)^2}{\sqrt{Q^2 - (\Omega/c)^2 - \mathrm{i}0}} \left(\delta_{\alpha\beta} - \frac{Q_\alpha Q_\beta}{(\Omega/c)^2} \right). \tag{32b}$$

Here, c is the speed of light in the medium surrounding the TMD heterostructure. We once again use the coordinate frame where the static excitonic polarization is $\boldsymbol{P} \parallel x$. We study the long-wavelength excitations and keep the leading order in $\hbar\Omega \ll E_B - E_g$ terms in the material relation (31): In this limit, only $P_{y,\boldsymbol{Q},\Omega}$ is nonzero and the self-consistency equation reads

$$2\pi_1(\Omega, \boldsymbol{Q}) D^E_{yy}(\Omega, \boldsymbol{Q}) = 1. \tag{33}$$

This equation determines the dispersion of the elementary excitations of the excitonic insulator $\mathcal{E}(\boldsymbol{Q})$ when light-matter interaction is fully taken into account. In the absence of condensate, our results (see Appendix D) are in complete agreement with the previous literature [13,38].

At $Q \to 0$, the dispersion is

$$\Omega \equiv \mathcal{E}(\boldsymbol{Q})/\hbar \approx c|Q_y|, \quad |Q_y| > \frac{c_s}{c} Q, \tag{34a}$$

where c_s is defined in Eq. (26). This expression is valid for practically all directions of $\boldsymbol{Q}$ apart from a small range of angles $\varphi = \angle(\boldsymbol{Q}, \boldsymbol{x})$, $\varphi < c_s/c$, where, for fixed Q, the y component of the wave vector becomes particularly small. For $\varphi = 0$ (i.e., $\boldsymbol{Q} \parallel x$), we find that

$$\Omega \equiv \mathcal{E}(\boldsymbol{Q})/\hbar = \xi Q^{3/2}, \quad Q \ll Q^* = \frac{c_s^2}{\xi^2}, \tag{34b}$$

$$\Omega \equiv \mathcal{E}(\boldsymbol{Q})/\hbar = c_s Q_x, \quad Q \gg Q^*, \tag{34c}$$

where $\xi = \hbar c_s c/[4\pi d_{\mathrm{exc}}^2 (E_B - E_g)]^{1/2}$. The dispersion of elementary excitations is shown in Fig. 4, with the focus on three key cases: (1) $\varphi = 0$ ($\boldsymbol{Q} \parallel x$), (2) the very small but nonzero case φ, where $c|Q_y| \ll c_s Q$, and (3) the case of $\varphi = \pi/2$ ($\boldsymbol{Q} \parallel y$) are presented in the respective panels of Fig. 4.

Naturally, if $|Q_y|$ is large enough the spectrum is linear and close to cQ_y asymptotics in Eq. (34a). This is a consequence of the fact that for sufficiently large $|Q_y|$ the excitations have significant longitudinal component of the dipole moment whose coupling with electromagnetic near field pushes their energy to light cone [see Fig. 4(c)]. This situation is similar to the case the two-dimensional plasmon in the presence of retardation [39,40]. We note that linear dispersion is generic for two-dimensional longitudinal excitons in quantum well structures and in atomically thin semiconductors; for excitons with a finite energy $E_x(\boldsymbol{Q} = 0) = E_g - E_B$, however, linear dispersion is only observed for states outside the light cone (Appendix D) [13,14,41,42]. Interestingly, even if $|Q_y|$ is small, the dispersion at $Q \to 0$ is still dominated by the light-matter interaction, as illustrated in Figs. 4(a) and 4(b). For instance, at $\varphi = 0$, the dispersion starts as $Q^{3/2}$ and turns over to the $c_s Q$ law typical for the Bogoliubov excitations only for wave vectors that exceed $Q_* \approx c_s^2/\xi^2$ [see Eqs. (34b) and (34c)]. For $|\varphi| \lesssim c_s/c$, the dispersion, as illustrated in Fig. 4(b), starts as $c|\sin\varphi|Q$, then turns to $Q^{3/2}$ asymptotics (34b), and with further increase in Q approaches the linear law (34c) dominated by the interactions in the condensate. In the relevant regime of small and intermediate Q, the

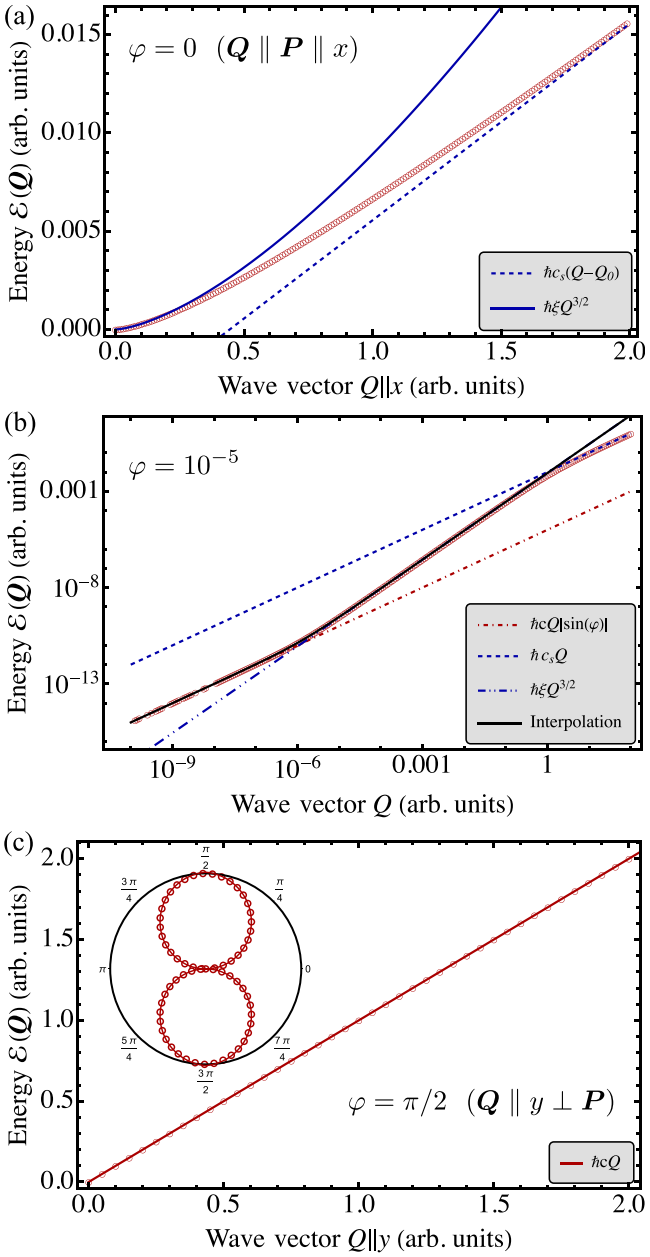

FIG. 4. Dispersion of elementary excitations of excitonic insulator with allowance for the light-matter coupling. Open red symbols show the dispersion calculated numerically solving Eq. (33); solid lines show analytical approximations; x axis corresponds to the polarization of the condensate $\boldsymbol{P} \parallel x$ (see text for details). (a) $\boldsymbol{Q} \parallel x$ ($\varphi = 0$). Dashed curve with $c_s Q$ asymptotics is shifted to allow for the Q-independent overall shift. (b) Small, but nonzero $\varphi = 10^{-5}$. Dot-dashed and dashed curves show Q-linear asymptotics [Eqs. (34a) and (34c)], blue dot-dot-dashed line shows $Q^{3/2}$ law [Eq. (34b)], and black solid line shows the interpolation [Eq. (35)]. (c) $\boldsymbol{Q} \parallel y$ ($\varphi = \pi/2$). Inset shows the angular dependence of the energy: Points correspond to the full Eq. (33) and the curve corresponds to Eq. (34a); small-φ deviations are not seen in the scale of the inset.

interpolation function

$$\mathcal{E}^2(\boldsymbol{Q}) = \hbar^2 c^2 Q^2 \sin^2\varphi + \hbar^2 \xi^2 Q^3, \quad \varphi \lesssim c_s/c, \tag{35}$$

rather accurately describes the results of numerical calculations, as shown by the black curve in Fig. 4(b). This nontrivial dispersion of Bogoliubov excitations is a result of the coupling of excitons to the electromagnetic field. The dispersion derived in Eq. (33) and shown in Fig. 4 deviates from the generic Bogoliubov dispersion given by Eq. (26) and indicates that the condensate fluctuations are qualitatively different.

The strong modification of the collective mode dispersion is somewhat similar to the Anderson-Higgs effect in superconductors [43–47]. We can understand the origin of this modification by considering the limit $|E_B - E_g| < kT$ and neglecting the exciton-exciton interactions and light-matter coupling: The exciton center-of-mass dispersion in this case is simply parabolic [Fig. 3(a)]. Upon taking into account coupling of excitons to the electromagnetic field, the longitudinal exciton dispersion would change from parabolic to linear [Eq. (D5a)], indicating that condensation is possible. When T is such that a condensate mean-field description is justified, the gapless collective Bogoliubov mode will have a $Q^{1/2}$ dispersion (cf. Ref. [48]). Although this consideration indicates the possibility of a true long-range order, the aforementioned $Q^{1/2}$ dispersion is not physical, since it lies above the light cone and violates causality. The proper analysis we have carried out shows that the excitations in the low Q excitations become lightlike and approach the light cone at $Q \to 0$. Correspondingly, these low-energy excitations contain a vanishing fraction of exciton character in the $Q \to 0$ limit, which in turn ensures suppression of thermal depletion of the condensate. Compared to the effect in superconductors where Cooper pairs are charged and their coupling with electromagnetic field pushes the dispersion up to the plasma frequency, the effect for neutral excitons is somewhat weaker: It stiffens the linear dispersion.

To verify that the thermal fluctuations do not destroy the condesate, we construct the Green's function of the center-of-mass motion of the excitons. In the presence of the light-matter coupling, the exciton susceptibility with respect to the electromagnetic field is renormalized compared to $\pi_1(\Omega, \boldsymbol{Q})$ due to the self-consistent interaction

$$\mathcal{G}(\Omega, \boldsymbol{Q}) = -\frac{1}{d_{\text{exc}}^2} \frac{\pi_1(\Omega, \boldsymbol{Q})}{1 - 2\pi_1(\Omega, \boldsymbol{Q}) D_{yy}^E(\Omega, \boldsymbol{Q})}. \tag{36}$$

Naturally, the poles of $\mathcal{G}$ correspond to the solutions of Eq. (33). The number of thermally excited excitons is given by [37]

$$N_{\text{exc}} = \sum_{\boldsymbol{Q}} \int \frac{d\Omega}{2\pi i} [\mathcal{G}(\Omega, \boldsymbol{Q}) - \mathcal{G}^*(\Omega, \boldsymbol{Q})] n(|\hbar\Omega|), \tag{37}$$

where

$$n(\hbar\Omega) = \frac{1}{\exp(\hbar\Omega/k_B T) - 1} \approx \frac{k_B T}{\hbar\Omega} \tag{38}$$

is the quasiparticle distribution function at T. The condensation in the strict sense of the term is possible if the integral converges at $Q \to 0$, i.e., if excited states host finite number of particles. To proceed, we express the Green's function in the vicinity of its poles as

$$\mathcal{G}(\Omega, \boldsymbol{Q}) = \frac{\mathcal{A}(\boldsymbol{Q})}{\Omega^2 - \mathcal{E}^2(\boldsymbol{Q}) - i0}, \tag{39}$$

with $\mathcal{A}(\boldsymbol{Q})$ denoting the quasiparticle weight. With this approximation, we find that

$$N_{\rm exc} = \sum_{\boldsymbol{Q}} \frac{\mathcal{A}(\boldsymbol{Q})}{\mathcal{E}(\boldsymbol{Q})} n[\mathcal{E}(\boldsymbol{Q})] \approx k_B T \sum_{\boldsymbol{Q}} \frac{\mathcal{A}(\boldsymbol{Q})}{\mathcal{E}^2(\boldsymbol{Q})}, \tag{40}$$

where in the last equality, the summation over $\boldsymbol{Q}$ should be cutoff at $\mathcal{E}(Q) \sim k_B T$. To verify that $N_{\rm exc}$ does not diverge, we derive an expression for $1/\mathcal{A}(\boldsymbol{Q})$ in the limit of small Q and φ:

$$\frac{1}{\mathcal{A}(\boldsymbol{Q})} = 1 + 2d_{\rm exc}^2 \frac{\partial}{\partial(\hbar\Omega)^2} D^E_{yy}(\Omega, \boldsymbol{Q})\Big|_{\Omega=\mathcal{E}(\boldsymbol{Q})}.$$

The quasiparticle weight $\mathcal{A}(\boldsymbol{Q})$ quantifies the exciton character of the elementary excitations. In the relevant range of small Q and φ, the factor $\mathcal{A}^{-1} = 4\pi d_{\rm exc}^2/Q$ yields

$$\mathcal{G}(\Omega, \boldsymbol{Q}) = \frac{(\hbar c)^2}{4\pi d_{\rm exc}^2} \frac{Q}{(\hbar\Omega)^2 - \mathcal{E}^2(\boldsymbol{Q}) - {\rm i}0}. \tag{41}$$

We emphasize that the factor Q appearing in the numerator of $\mathcal{G}(\Omega, \boldsymbol{Q})$ indicates the vanishing quasiparticle weight $\mathcal{A}(Q) \to 0$ of the collective excitations as $Q \to 0$. Using the small-Q and small-φ asymptotics, we obtain

$$N_{\rm exc} = \frac{2ck_BT}{\sqrt{3}(2\pi)^2 d_{\rm exc}^2} \times \left(\frac{k_BT}{\hbar\xi^4}\right)^{1/3}. \tag{42}$$

Remarkably, there is a finite number of thermally excited excitons at finite T, demonstrating that light-matter coupling ensures Bose-Einstein condensation of ground-state interlayer excitons.

The aforementioned results stand in contrast to what one finds in the absence of the light-matter interaction ($d_{\rm exc} \equiv 0$): It follows from Eqs. (27a) and (36) that

$$\mathcal{G}(\Omega, \boldsymbol{Q}) \approx \frac{E_B - E_g}{(\hbar\Omega)^2 - c_s^2 Q^2 - {\rm i}0}, \tag{43a}$$

which for two-dimensional excitons gives

$$N_{\rm exc} \propto \sum_{\boldsymbol{Q}} \frac{k_BT}{Q} \frac{1}{Q} \to \text{diverges}, \tag{43b}$$

indicating that thermal fluctuations deplete the condensate [37].

The analysis of the excitation spectra [Eqs. (33)–(35)] and of the condensate depletion [Eqs. (37)–(42)] accounts for the contribution of states with $Q \to 0$. Indeed, these long-wavelength fluctuations destroy long-range order in two-dimensional systems. Our analysis shows that the light-matter interaction suppresses such fluctuations and stabilizes the long-range order in the exciton condensate.

The wave-vector scale Q^* in Eqs. (34b) and (34c) controls the transition of the excitation dispersion from the light-matter interaction dominated dispersion, Eq. (34b) at $Q \ll Q^*$, to the interaction dominated dispersion, Eq. (34c) at $Q \gg Q^*$. Correspondingly, the length scale $R^* = 1/Q^*$ associated with this wave vector controls the spatial correlations of the condensates phase fluctuations: In agreement with above, for $r \gg R^*$ the condensate phase correlator approaches a constant value corresponding to the true long-range order in our system and finite fraction of excitons in thermally excited states $N_{\rm exc}$ in Eq. (42). For $r \ll R^*$ (but $r \gg \hbar/\sqrt{Mk_BT}$), the phase correlator is a logarithmic function of distance, indicating algebraic long-range order expected for the BKT transition.

Roughly, the energy $\mathcal{E}^*(Q^*) \sim \hbar c_s^2/\xi^2$ sets the temperature scale $k_BT_c \sim \mathcal{E}^*(Q^*) \ll T_{\rm BKT}$ below which the energies of typical excitations are dominated by the light-matter interaction. It can be argued that at $T \ll T_c$ the phase fluctuations of condensate are suppressed by the light-matter coupling and the system shows the true long-range order. Precise evaluation of the condensation temperature, T_c, is a highly involved problem that is beyond the scope of our paper, as it requires knowledge of excitation spectra not only in the limit of $T \to 0$ derived above, but across a finite temperature range up to the pairing temperature $T_{\rm pair}$ [49,50]. Note that for considered R-stacked heterobilayer the magnetic field of 5 T produces the valley Zeeman splitting for bright intervalley excitons of about $E_Z = g\mu_B B \approx 1.7$ meV for the realistic exciton g factor of 6 for, e.g., $MoSe_2/WSe_2$ structure [51]. Hence, for the temperatures below $T_Z = E_Z/k_B \approx 20$ K, only one bright valley can be relevant. The analysis of the $K - K'$ and $K - Q$ excitons in heterobilayers [52] is beyond the scope of this work.

We stress that the results related to the long-range order have fundamental significance: We demonstrate a clear physical mechanism that provides, contrary to the common wisdom, a long-range order in two-dimensional systems with broken continuous symmetry.

Nevertheless, in state-of-the-art finite-size samples, the effect of the long-range fluctuations on excitonic insulator is suppressed simply because of the finite size of the flake. Correspondingly, the condensation is possible because all excitations become gapped [49,53]. For the same reason, inevitable disorder related to the defects, local strain, and twist angle fluctuations in heterobilayers, which results in exciton localization, enables exciton condensation in disordered two-dimensional systems, but without formation of the long-range order [54].

V. EXPERIMENTAL SIGNATURES

The search for the smoking gun evidence of the excitonic insulator formation is one of the outstanding challenges in the field. As a necessary but not sufficient first step, one could probe the presence of spontaneously generated ground-state excitons through detection of the $1s$–$2p$ dipole-active intraexciton transition [55]. We envisage a simple experiment where the tetrahertz absorption spectrum is measured as a function of the bias voltage which varies E_g–E_B: The onset of the tetrahertz absorption demonstrates the spontaneous formation of excitons in the system.

Generally, the formation of the ordered state can be detected using optical spectroscopy since ferroelectric order should change the selection rules for transitions from purely circular to elliptical. Figure 5 details the generic TMD band structure where $c+2$ remote conduction band has an opposite C_3 angular momentum compared to the conduction band [56,57]. The optical transitions from the valence band v to the $c+2$ conduction band of the opposite monolayer in the K_+ valley are σ^- circular polarized, while the transitions from the bottom conduction band c to $c+2$ in the same monolayer are σ^+ circularly polarized [Fig. 5(a)]. The so-called

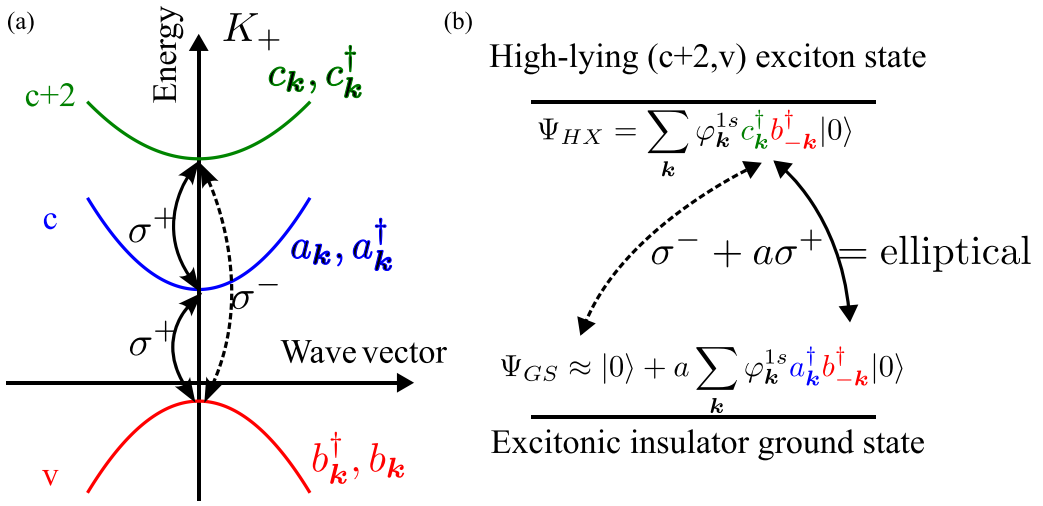

FIG. 5. Detection of the exciton insulator state with the ferroelectric order. (a) Schematics of the TMD heterobilayer band structure in the K_+ valley that shows the nearest valence and conduction bands, as well as the remote $c+2$ band with chirality that is opposite to that of the c-band chirality. The selection rules for the interband transitions are shown by arrows. (b) Interference of transitions for excitation or recombination of the high-lying exciton associated with the remote conduction band. In the presence of excitonic condensate, $a \neq 0$, the selection rules for such transitions involve elliptical polarization.

"high-lying" excitonic transitions associated with this remote band have already been observed and studied both for mono- and bilayer structures [58–60].

The ground state in the presence of an excitonic insulator and ferroelectric order is a mixture of the "vacuum" state $|0\rangle$ and the exciton Fock states $|1\rangle$, $|2\rangle$, etc. [Eq. (15)]. If we focus on the $1s$ exciton transition between the ground state in Eq. (15) and the $c+2$ band, as shown in Fig. 5(b), we notice that there are two pathways for this transition: from $|0\rangle$ by σ^- photon or from $|1\rangle$ by σ^+ photon. Consequently, this transition will generally be elliptically polarized and the polarization axis will be linked to the phase of the condensate's order parameter a. The magnitude of linear polarization is proportional to $|a|$. The oscillator strength of the transition $v \leftrightarrow c+2$ (active in the σ^- polarization) can be relatively weak compared to that of $c \leftrightarrow c+2$, since it involves the interlayer transfer of the hole. However, in the regime where condensate order parameter $|a|$ is small as well, the degree of elliptical polarization of the optical transition can be quite sizable.

The emergence of ferroelectric order in interlayer excitons may also be detected by intralayer exciton spectroscopy. It has been predicted and experimentally demonstrated that the presence of interlayer excitons leads to the formation of attractive and repulsive polaron branches in optically active intralayer excitonic resonances [61]. The attractive polaron (AP) in this case can be considered as a collective excitation of biexcitons—bound state of an intra- and interlayer exciton [61]. By measuring the polarization dependence of the AP branch in each layer, it is also possible to determine the valley degree of freedom of both the electron and the hole forming the interlayer exciton; for example, if the interlayer excitons are bound K_+-valley electron-hole pairs, then the AP resonances of both layers would be right-hand circularly polarized.

Upon condensation and formation of the ferroelectric order, we could expect the polarization properties of AP resonances to be modified. In the limit where the biexciton radius is smaller than the average separation between ground-state interlayer excitons, the biexcitons would have a finite electric dipole moment along the same axis as the condensate, which should lead to linearly polarized AP resonance. The effect is related to previous reports of linearly polarized excitonic resonances observed upon formation of nematic order of electrons [62]. By measuring the linear polarization axis of AP across the sample, it should be possible to determine the correlation length of the ferroelectric order.

VI. OUTLOOK

Dipolar 2D interlayer excitons in van der Waals heterostructures have emerged as a new platform for investigation of strongly correlated bosons in the solid state. While experiments have already demonstrated perfect drag and Wigner crystal states of finite-energy excitons, outstanding theoretical proposals range from exciton mediated superconductivity [63,64] to bosonic fractional Chern insulators [65,66]. Even though in the short run the experiments are likely to be carried out in small systems where the distinction between the power-law decay of the correlations and the true long-range order of the parent excitonic insulator state would not be discernible, our findings are important not only for future experiments but also for our understanding of the possibilities in the exciting platform of 2D materials.

We also highlight a connection to 2D XXZ magnets, where it is well known that a ferromagnetic phase transition that breaks the U(1) symmetry is possible due to flip-flop magnetic dipole interactions. The precise connection between the two problems, as well as the role of long-range dipolar interactions between ground-state excitons, will be the subject of future work.

Even though vacuum electromagnetic field fluctuations lead to observable effects such as the Lamb shift or the Casimir effect, an interesting open question in condensed

matter physics is whether the functionality of a quantum material can be modified through coupling to cavity-enhanced vacuum fields [67]. While we do not assume a cavity structure, we show here that the coupling of elementary excitations to the vacuum field leads to a qualitative change in the ground state of a 2D material by inducing a paraelectric-to-ferroelectric phase transition. Naturally, enhancement of vacuum fluctuations at vanishing energies would lead to a higher T_c and a more robust ferroelectric state, similar to the proposals of Higgs mode stabilization in superconductors [68].

VII. CONCLUSION

We showed that true long-range ferroelectric order and Bose-Einstein condensation of interlayer excitons can occur in two-dimensional heterobilayer semiconductors, despite the restrictions imposed by the Mermin-Wagner theorem. The key requirements include reducing the interlayer band gap below the exciton binding energy via an applied electric field, applying a finite magnetic field to lift the valley degeneracy, and having a band structure that supports long-range electron-hole exchange interaction. Under these conditions, excitons spontaneously form in the ground state and acquire a photon-like linear dispersion at small momenta due to coupling with the electromagnetic field, which suppresses phase fluctuations and stabilizes the condensate at finite temperatures.

The excitonic insulator phase is characterized by spontaneous breaking of U(1) symmetry, leading to a ferroelectric state with in-plane electric polarization. The coexistence of superfluidity and ferroelectricity in this system represents an electronic ground state enabled by vacuum fluctuations. The findings establish dipolar 2D interlayer excitons as a promising platform for exploring strongly correlated bosonic phases and suggest that cavity-enhanced vacuum fields could further stabilize the ferroelectric order, opening possibilities for controlling quantum material functionality through light-matter coupling.

ACKNOWLEDGMENTS

The authors acknowledge insightful discussions with Allan MacDonald, Peter Littlewood, Andrew Millis, Ivan Iorsh, and Eugene Demler. They also thank Anna Seiler for sharing Fig. 1. M.M.G. was supported by the RSF Grant No. 23-12-00142-Continuation. A.İ. was supported by the Swiss National Science Foundation (SNSF) under Grant No. 2000-1-240035.

DATA AVAILABILITY

The work presented in this work is theoretical and analytical. There are no data associated with it.

APPENDIX A: DERIVATION OF THE 2 × 2 HAMILTONIAN

We assume that the tunneling is allowed between the two conduction (valence) bands of the two layers but that there is no interband tunneling. Consequently, the interlayer hybridization results from the valence band 1–valence band 2 and conduction band 1–conduction band 2 tunnel couplings. The 4×4 Hamiltonian describing orbital states (without Coulomb interaction) reads

$$\mathcal{H}_4 = \begin{pmatrix} E_{c1}(\boldsymbol{k}) & \gamma_\alpha^1 k_\alpha & t_{cc} & 0 \\ \gamma_\alpha^{1,*} k_\alpha & E_{v1}(\boldsymbol{k}) & 0 & t_{vv} \\ t_{cc}^* & 0 & E_{c2}(\boldsymbol{k}) & \gamma_\beta^{2,*} k_\beta \\ 0 & t_{vv}^* & \gamma_\beta^2 k_\beta & E_{v2}(\boldsymbol{k}) \end{pmatrix}. \tag{A1}$$

Here, the 2×2 blocks correspond to the first and second layers, $E_{c1}(\boldsymbol{k}) = E_{c1} + \hbar^2 k^2/2m_c$ ($E_{c2}(\boldsymbol{k}) = E_{c2} + \hbar^2 k^2/2m_c$) and $E_{v1}(\boldsymbol{k}) = E_{v1} + \hbar^2 k^2/2m_v$ ($E_{v2}(\boldsymbol{k}) = E_{v2} + \hbar^2 k^2/2m_v$) are the "bare" electron dispersions in the conduction and valence bands of the first (second) layer, respectively. $E_{c1}(\boldsymbol{k})$ ($E_{c2}(\boldsymbol{k})$) and $E_{v1}(\boldsymbol{k})$ ($E_{v2}(\boldsymbol{k})$) are the conduction and valence band energies with the effective masses m_c and m_v determined by couplings to other remote bands that are not described by the Hamiltonian of Eq. (1). The parameters t_{cc} and t_{vv} describe the interlayer tunneling strength and $\gamma_\alpha^1 k_\alpha$, $\gamma_\beta^2 k_\beta$ describe the $\boldsymbol{k} \cdot \boldsymbol{p}$ mixing of the conduction and valence bands in the corresponding layers, with $\alpha, \beta = x, y$ denoting the Cartesian components, and γ_α^1, γ_β^2 are the interband momentum matrix elements multiplied by $\hbar/m_0$ (m_0 is the free electron mass). Hereafter, the summation over the repeated subscripts is implicitly assumed. For $K_\pm$ valleys, $\gamma_\alpha^{1,2} k_\alpha = \hbar p_{cv}^{1,2}/m_0 (k_x \mp \mathrm{i} k_y)$. The interband matrix elements $p_{cv}^{1,2}$ can be made real by the choice of the wavefunction phases.

Assuming that in the relevant wave-vector range $E_{ci} - E_{vi} \gg |\gamma_\alpha^i k_\alpha|$ $(i = 1, 2)$, $|E_{c1} - E_{c2}| \gg |t_{cc}|$, and $|E_{v1} - E_{v2}| \gg |t_{vv}|$, we use perturbation theory to reduce the full Hamiltonian to the 2×2 matrix describing the nearest conduction $c1$ and valence $v2$ band states given by Eq. (1). The parameters in this Hamiltonian are explicitely given by

$$E_c(\boldsymbol{k}) = E_c + \frac{\hbar^2 k^2}{2m_c} + \frac{|t_{cc}|^2}{E_{c1} - E_{c2}} + \frac{|\gamma_\alpha^1 k_\alpha|^2}{E_{c1} - E_{v1}} = \frac{E_g}{2} + \frac{\hbar^2 k^2}{2m_e}, \tag{A2a}$$

$$E_v(\boldsymbol{k}) = E_v + \frac{\hbar^2 k^2}{2m_v} + \frac{|t_{vv}|^2}{E_{v2} - E_{v1}} + \frac{|\gamma_\alpha^2 k_\alpha|^2}{E_{v2} - E_{c2}} = -\frac{E_g}{2} - \frac{\hbar^2 k^2}{2m_h}, \tag{A2b}$$

$$\gamma_\alpha k_\alpha = \frac{\gamma_\alpha^1 k_\alpha t_{vv}}{2} \left(\frac{1}{E_{c1} - E_{v1}} + \frac{1}{E_{v2} - E_{v1}} \right) + \frac{\gamma_\alpha^{2,*} k_\alpha t_{cc}}{2} \left(\frac{1}{E_{c1} - E_{c2}} + \frac{1}{E_{v2} - E_{c2}} \right). \tag{A2c}$$

Here, $m_e, m_h > 0$ are the effective masses of the electrons and holes in the absence of interlayer coupling, E_g is the effective band gap, and γ_α are the effective interband momentum matrix elements.

APPENDIX B: EXCITON INSTABILITY AT FINITE TEMPERATURE

We consider a simplified version of a pairing for the short-range interaction, $V_{k-k'} \equiv V_0$, and symmetric dispersions of electrons and holes, $E_e(\boldsymbol{k}) = E_h(-\boldsymbol{k})$. In this case, $\Delta_k = \Delta$.

The gap equation with allowance for the finite T can be written as (cf. Ref. [37])

$$\frac{1}{V_0} = \sum_{\boldsymbol{k}} \frac{1-2n_{\boldsymbol{k}}}{2\xi_{\boldsymbol{k}}}, \tag{B1}$$

where

$$\xi_{\boldsymbol{k}} = \mathcal{E}_{\boldsymbol{k}}/2 = \sqrt{E_e^2(\boldsymbol{k}) + \Delta^2}$$

and

$$n_{\boldsymbol{k}} = \frac{1}{\exp\left(\xi_{\boldsymbol{k}}/k_BT\right)+1},$$

where k_BT is the temperature expressed in the units of energy. Removing high-energy divergencies in Eq. (B1) in a standard way and expressing V_0 via the bound-state binding energy E_B, we arrive at the gap equation in the following form:

$$\ln\left(E_B\frac{\sqrt{E_g^2+4\Delta^2}-E_g^2}{2\Delta^2}\right) = 2\int_0^\infty \frac{dx}{\sqrt{(E_g/2+x)^2+\Delta^2}\exp\left(\frac{\sqrt{(E_g/2+x)^2+\Delta^2}}{k_BT}\right)+1}. \tag{B2}$$

At $T=0$, the right-hand side of Eq. (B2) vanishes. For small $E_B - E_g \ll E_B$ the gap, $\Delta \ll E_B, E_g$ (hereafter in this section we select arbitrary phase of the gap to be zero for definiteness). Keeping the leading order terms in Δ/E_B, we obtain

$$\Delta = \begin{cases} \sqrt{E_B(E_B-E_g)}, & E_B > E_g, \\ 0, & \text{otherwise.} \end{cases} \tag{B3}$$

This result is in agreement with Eq. (14). This dependence is illustrated in Fig. 6(a): Solid red curve shows the gap dependence found numerically from Eq. (B2) and dotted magneta curve shows Eq. (B3).

In the relevant temperature range $k_BT \ll E_g, E_B$. It allows to evaluate integral in the right-hand side of Eq. (B2) as

$$2\int_0^\infty \frac{dx}{\sqrt{(E_g+x)^2+\Delta^2}\exp\left(\frac{\sqrt{(E_g+x)^2+\Delta^2}}{k_BT}\right)+1} \approx -2\mathrm{Ei}(-E_g/k_BT) \approx \frac{2k_BT}{E_g}e^{-E_g/k_BT}, \tag{B4}$$

where $\mathrm{Ei}(z) = -\int_{-z}^{\infty} e^{-t}/t\,dt$ is the exponential integral. Naturally, at finite T the gap is reduced and the instability point shifts to smaller values of E_g compared to the zero T case of $E_B = E_g$. The gap as a function of T is shown in Fig. 6(b), where dots demonstrate full numerical solution of Eq. (B2) and the solid lines represent the analytical result obtained using the second approximation in Eq. (B4):

$$\Delta = \sqrt{2\tilde{E}_B(T)(\tilde{E}_B(T)-E_g)}, \tag{B5}$$

where

$$\tilde{E}_B(T) = E_B\exp\left(\frac{4k_BT}{E_g}e^{-E_g/2k_BT}\right).$$

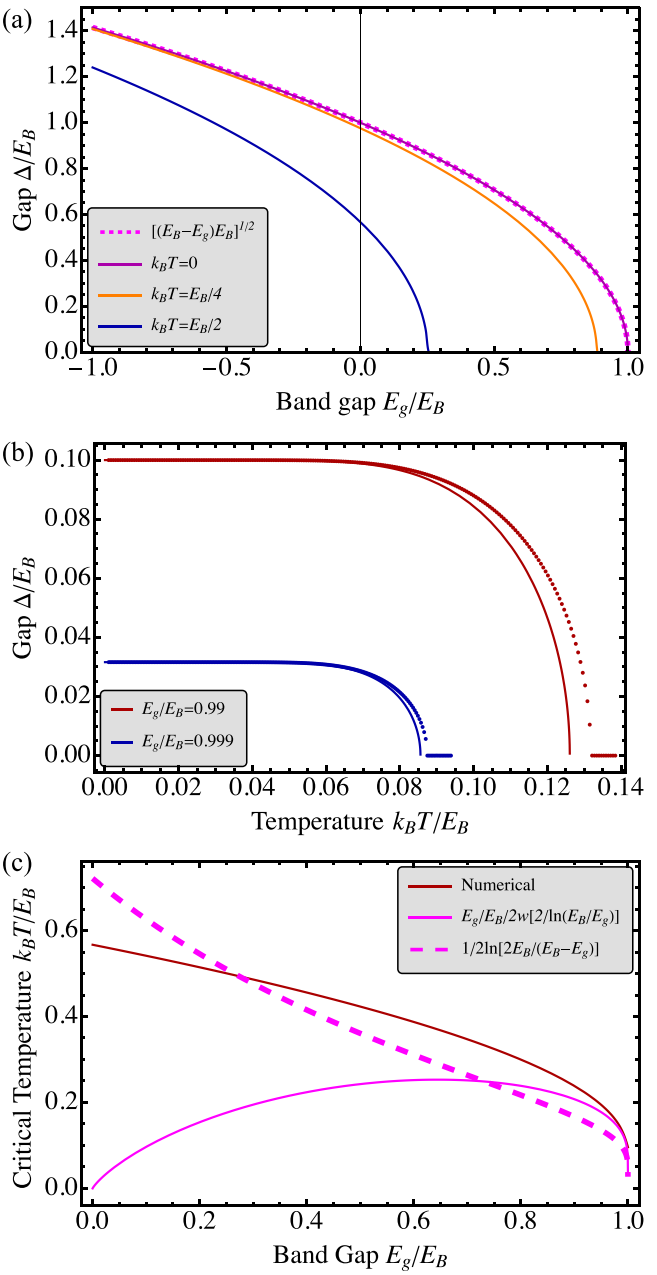

FIG. 6. Pairing gap Δ as a function of the ratio E_g/E_B [panel (a)] and temperature k_BT. (c) Critical temperature for the pairing T_{pair} as a function of the ratio E_g/E_B. See legends and text for details.

This approximation works better the closer E_g is to E_B, i.e., the smaller the gap is.

Setting $\Delta = 0$, we obtain from Eq. (B2) the critical temperature of pairing, solid red line in Fig. 6(c). Analytical approximations found from Eq. (B5): $E_B(T_{\text{pair}}) = E_g$ are shown by the solid magneta line (where the solution of this equation is expressed via the Lambert-w function or product logarithm) and dashed magneta line where a crude logarithmic approximation

$$T_{\text{pair}} = \frac{E_g}{2k_B}\frac{1}{\ln[2E_B/(E_B-E_g)]} \tag{B6}$$

has been employed. It is noteworthy that the critical temperature evaluated in this way corresponds to the critical temperature of the pairing. There are fluctuations of the phase of Δ (bosonic Goldstone mode) that affect the condensate and would destroy the long-range order in the system in the absence of coupling to the electromagnetic field (see the main text).

APPENDIX C: DERIVATION OF GAP EQUATION BY UNITARY TRANSFORM

Following Ref. [28], it is convenient to perform a transformation to the novel operators

$$a_{\boldsymbol{k}} \to u_{\boldsymbol{k}} a_{\boldsymbol{k}} + v_{\boldsymbol{k}} b^{\dagger}_{-\boldsymbol{k}}, \quad a^{\dagger}_{\boldsymbol{k}} \to u_{\boldsymbol{k}} a^{\dagger}_{\boldsymbol{k}} + v^{*}_{\boldsymbol{k}} b_{-\boldsymbol{k}}, \tag{C1a}$$

$$b_{-\boldsymbol{k}} \to u_{\boldsymbol{k}} b_{-\boldsymbol{k}} - v_{\boldsymbol{k}} a^{\dagger}_{\boldsymbol{k}}, \quad b^{\dagger}_{-\boldsymbol{k}} \to u_{\boldsymbol{k}} b^{\dagger}_{-\boldsymbol{k}} - v^{*}_{\boldsymbol{k}} a_{\boldsymbol{k}}, \tag{C1b}$$

where

$$u^2_{\boldsymbol{k}} + |v_{\boldsymbol{k}}|^2 = 1,$$

and it is convenient to parametrize $u_{\boldsymbol{k}}$ and $v_{\boldsymbol{k}}$ via the so far unknown function $\varphi(\boldsymbol{k})$:

$$u_{\boldsymbol{k}} = \cos\varphi(\boldsymbol{k}) \approx 1 - \frac{|\varphi(\boldsymbol{k})|^2}{2},$$

$$v_{\boldsymbol{k}} = \mathrm{i}e^{\mathrm{i}\arg\varphi(\boldsymbol{k})}\sin\varphi(\boldsymbol{k}) \approx \mathrm{i}\left(1 - \frac{|\varphi(\boldsymbol{k})|^2}{6}\right)\varphi(\boldsymbol{k}). \tag{C1c}$$

It is instructive to present

$$u_{\boldsymbol{k}} v_{\boldsymbol{k}} \approx \mathrm{i}\varphi(\boldsymbol{k})\left[1 - \tfrac{2}{3}|\varphi(\boldsymbol{k})|^2\right], \tag{C1d}$$

$$u^2_{\boldsymbol{k}} - |v_{\boldsymbol{k}}|^2 \approx 1 - 2|\varphi(\boldsymbol{k})|^2. \tag{C1e}$$

Note that the actual unitary transformation is provided by the operator

$$S = \exp\left\{\mathrm{i}\sum_{\boldsymbol{k}}\left[\varphi(\boldsymbol{k})a^{\dagger}_{\boldsymbol{k}}b^{\dagger}_{-\boldsymbol{k}} - \varphi^{*}(\boldsymbol{k})b_{-\boldsymbol{k}}a_{\boldsymbol{k}}\right]\right\}.$$

The choice of real $u_{\boldsymbol{k}}$ is a matter of convenience. Function $\varphi(\boldsymbol{k})$ plays a role of the order parameter; it describes the electron-hole correlations in the system's ground state.

The transformed Hamiltonian takes the form up to $\propto \varphi^3(\boldsymbol{k})$ terms (operator-independent part is omitted):

$$\mathcal{H} = S^{\dagger}(\mathcal{H}_2 + \mathcal{V})S = \sum_{\boldsymbol{k}} \mathcal{E}_e(\boldsymbol{k})a^{\dagger}_{\boldsymbol{k}}a_{\boldsymbol{k}} + \mathcal{E}_h(\boldsymbol{k})b^{\dagger}_{\boldsymbol{k}}b_{\boldsymbol{k}} + \mathcal{T} + \mathcal{M} + \tilde{\mathcal{V}}, \tag{C2}$$

with the renormalized electron and hole dispersions

$$\mathcal{E}_e(\boldsymbol{k}) = E_e(\boldsymbol{k}) - |\varphi(\boldsymbol{k})|^2[E_e(\boldsymbol{k}) + E_h(-\boldsymbol{k})] + (u_{\boldsymbol{k}}v^{*}_{\boldsymbol{k}}\gamma_{\alpha}k_{\alpha} - u_{\boldsymbol{k}}v_{\boldsymbol{k}}\gamma^{*}_{\alpha}k_{\alpha}) - \cdots, \tag{C3a}$$

$$\mathcal{E}_h(\boldsymbol{k}) = E_h(\boldsymbol{k}) - |\varphi(\boldsymbol{k})|^2[E_e(-\boldsymbol{k}) + E_h(\boldsymbol{k})] - (u_{\boldsymbol{k}}v^{*}_{\boldsymbol{k}}\gamma_{\alpha}k_{\alpha} - u_{\boldsymbol{k}}v_{\boldsymbol{k}}\gamma^{*}_{\alpha}k_{\alpha}) - \cdots, \tag{C3b}$$

renormalized interband coupling

$$\mathcal{T} = \sum_{\boldsymbol{k}} \gamma_{\alpha}k_{\alpha}(1 - |\varphi(\boldsymbol{k})|^2)a^{\dagger}_{\boldsymbol{k}}b^{\dagger}_{-\boldsymbol{k}} + \gamma^{*}_{\alpha}k_{\alpha}\varphi^2(\boldsymbol{k})a^{\dagger}_{\boldsymbol{k}}b^{\dagger}_{-\boldsymbol{k}} + \mathrm{H.c.} = \sum_{\boldsymbol{k}} \lambda_{\boldsymbol{k}}a^{\dagger}_{\boldsymbol{k}}b^{\dagger}_{-\boldsymbol{k}} + \lambda^{*}_{\boldsymbol{k}}b_{-\boldsymbol{k}}a_{\boldsymbol{k}}, \tag{C4}$$

renormalized interaction $\tilde{\mathcal{V}}$ containing four normally ordered creation and annihilation operators and, finally, "dangerous" terms that contain two creation or two annihilation operators stemming from both the dispersion and interactions:

$$\mathcal{M} = \sum_{\boldsymbol{k}} M_{\boldsymbol{k}}a^{\dagger}_{\boldsymbol{k}}b^{\dagger}_{-\boldsymbol{k}} + M_{\boldsymbol{k}}b_{-\boldsymbol{k}}a_{\boldsymbol{k}}, \tag{C5}$$

where

$$M_{\boldsymbol{k}} = \underbrace{\mathrm{i}\varphi(\boldsymbol{k})\left[1 - \frac{2}{3}|\varphi(\boldsymbol{k})|^2\right][E_e(\boldsymbol{k}) + E_h(-\boldsymbol{k})]}_{\text{free particle dispersion}\propto u_{\boldsymbol{k}}v_{\boldsymbol{k}}} - \mathrm{i}\sum_{\boldsymbol{k}'} \underbrace{V_{\boldsymbol{k}-\boldsymbol{k}'}\left[1 - 2|\varphi(\boldsymbol{k})|^2 - \frac{2}{3}|\varphi(\boldsymbol{k}')|^2\right]\varphi(\boldsymbol{k}')}_{\text{electron-hole attraction}\propto u_{\boldsymbol{k}'}v_{\boldsymbol{k}'}(u^2_{\boldsymbol{k}}-|v_{\boldsymbol{k}}|^2)} + \underbrace{V_{\boldsymbol{k}-\boldsymbol{k}'}2\varphi(\boldsymbol{k})|\varphi(\boldsymbol{k}')|^2}_{\text{e-e and e-h repulsion}}. \tag{C6}$$

These $\mathcal{M}$ contributions lead to the exciton instability.

The order parameter can be found from the condition that, in the ground state, the contributions that spontaneously give rise to electrons and holes vanish [25,28,69]. Neglecting exciton-exciton interactions, we have the condition of vanishing "dangerous" terms in the form

$$\lambda_{\boldsymbol{k}} + M_{\boldsymbol{k}} = 0. \tag{C7}$$

In this case of absence interband coupling, $\lambda_{\boldsymbol{k}} = 0$, naturally, one solution of homogeneous Eq. (C7) corresponds to $\varphi(\boldsymbol{k}) \equiv 0$ (no order parameter). A nontrivial solution is possible and can be found iteratively, assuming that $|\varphi(\boldsymbol{k})| \ll 1$.

First approximation. We keep only $\varphi(\boldsymbol{k})$-linear terms in Eq. (C6) and obtain

$$0 = [E_e(\boldsymbol{k}) + E_h(-\boldsymbol{k})]\varphi(\boldsymbol{k}) - \sum_{\boldsymbol{k}'} V_{\boldsymbol{k}-\boldsymbol{k}'}\varphi(\boldsymbol{k}') \tag{C8}$$

or

$$0 = \left[E_g + \frac{\hbar^2k^2}{2\mu}\right]\varphi(\boldsymbol{k}) - \sum_{\boldsymbol{k}'} V_{\boldsymbol{k}-\boldsymbol{k}'}\varphi(\boldsymbol{k}'), \tag{C9}$$

where $\mu = m_e m_h/(m_e + m_h)$ is the electron-hole reduced mass. It can be assumed that $\varphi(\boldsymbol{k}) = a\varphi^{1s}_{\boldsymbol{k}}$, where $\varphi^{1s}_{\boldsymbol{k}}$ is the (normalized) exciton wavefunction corresponding to the lowest in the energy bound state with the energy $E_0 = -E_B$, where $E_B > 0$ is the exciton binding energy:

$$\frac{\hbar^2k^2}{2\mu}\varphi^{1s}_{\boldsymbol{k}} - \sum_{\boldsymbol{k}'} V_{\boldsymbol{k}-\boldsymbol{k}'}\varphi^{1s}_{\boldsymbol{k}} = -E_B\varphi^{1s}_{\boldsymbol{k}}. \tag{C10}$$

In this way, for $E_g = E_B$, Eq. (C9) has nontrivial solution.

Second approximation. We next show that for $E_g < E_B$ the nontrivial solution is present as well. Keeping cubic terms, we obtain

$$\left[E_g + \frac{\hbar^2k^2}{2\mu}\right]\varphi(\boldsymbol{k}) - \sum_{\boldsymbol{k}'} V_{\boldsymbol{k}-\boldsymbol{k}'}\varphi(\boldsymbol{k}') = \mathcal{F}^{(3)}_{\boldsymbol{k}}\{\varphi\}, \tag{C11}$$

where the functional

$$\mathcal{F}_{\boldsymbol{k}}^{(3)}\{\varphi\} = \frac{2}{3}\left[E_g + \frac{\hbar^2 k^2}{2\mu}\right]|\varphi(\boldsymbol{k})|^2\varphi(\boldsymbol{k}) + \sum_{\boldsymbol{k}'} V_{\boldsymbol{k}-\boldsymbol{k}'}\left[2\varphi(\boldsymbol{k})\varphi^*(\boldsymbol{k}') - 2|\varphi(\boldsymbol{k})|^2 - \frac{2}{3}|\varphi(\boldsymbol{k}')|^2\right]\varphi(\boldsymbol{k}'). \tag{C12}$$

It is convenient to simplify these equations making formal replacement

$$\varphi(\boldsymbol{k}) \to \varphi(\boldsymbol{k})\left[1 - \tfrac{2}{3}|\varphi(\boldsymbol{k})|^2\right]. \tag{C13}$$

Equation (C11) remains, while the functional takes a simpler form

$$\mathcal{F}_{\boldsymbol{k}}^{(3)}\{\varphi\} = 2\sum_{\boldsymbol{k}'} V_{\boldsymbol{k}-\boldsymbol{k}'}\varphi(\boldsymbol{k})[\varphi^*(\boldsymbol{k}') - \varphi^*(\boldsymbol{k})]\varphi(\boldsymbol{k}'). \tag{C14}$$

Formal solution of Eq. (C11) can be written via the Green's function of the exciton $G_{\rm exc}(\boldsymbol{k};\varepsilon)$:

$$\varphi(\boldsymbol{k}) = -\sum_{\boldsymbol{k}'} G_{\rm exc}(\boldsymbol{k}-\boldsymbol{p};-\Delta)\mathcal{F}_{\boldsymbol{p}}^{(3)}, \tag{C15}$$

where

$$\left[-\varepsilon + \frac{\hbar^2 k^2}{2\mu}\right]G_{\rm exc}(\boldsymbol{k}-\boldsymbol{p};\varepsilon) - \sum_{\boldsymbol{k}'} V_{\boldsymbol{k}-\boldsymbol{k}'}G_{\rm exc}(\boldsymbol{k}'-\boldsymbol{p};\varepsilon) = -\delta_{\boldsymbol{k},\boldsymbol{p}}. \tag{C16}$$

To find the ground state, we set

$$\varphi(\boldsymbol{k}) = |a|e^{i\chi}\varphi_{\boldsymbol{k}}^{1s} \tag{C17}$$

and take into account the cubic-in-φ contributions in $M_{\boldsymbol{k}}$. For $M_{\boldsymbol{k}}$ in the form of Eq. (C6), it turns out that the phase χ is arbitrary, while a can be found from the nonlinear equation

$$0 = \sum_{\boldsymbol{k}}\left(\varphi_{\boldsymbol{k}}^{1s}\right)^* M_{\boldsymbol{k}} \;\Rightarrow\; (E_g - E_B)|a| = -g|a|^3, \tag{C18}$$

where the constant g is given as

$$g = 2\sum_{\boldsymbol{k}}\left(\varphi_{\boldsymbol{k}}^{1s}\right)^*\mathcal{F}_3^{(3)}\{\varphi_{\boldsymbol{k}}^{1s}\} = \sum_{\boldsymbol{k}}\left(E_B + \frac{\hbar^2 k^2}{2\mu}\right)|\varphi_{\boldsymbol{k}}^{1s}|^4 - 2\sum_{\boldsymbol{k},\boldsymbol{k}'} V_{\boldsymbol{k}-\boldsymbol{k}'}|\varphi_{\boldsymbol{k}}^{1s}|^2|\varphi_{\boldsymbol{k}'}^{1s}|^2. \tag{C19}$$

In derivation of Eq. (C19), we made use of the fact that function $\varphi_{\boldsymbol{k}}^{1s}$ obeys Eq. (C10). One can check that $g > 0$ and show that an order of magnitude estimate gives $g \sim a_B^2 E_B$. Equations (C18) and (C19) agree with Ref. [28]. The result presented in the main text, Eq. (13), corresponds to the first term in the second line Eq. (C19).

APPENDIX D: EXCITON DISPERSION IN THE PRESENCE OF LIGHT-MATTER INTERACTION

It is instructive to establish a link between the results obtained in the main text and well-known effect of the exciton longitudinal-transverse splitting in two-dimensional systems [12–14,38,41,42]. We start from a noncondensed isotropic case. In this situation, it is convenient to use the basis of the transversal and longitudinal exciton modes with $\boldsymbol{P} \parallel \boldsymbol{Q}$ and $\boldsymbol{P} \perp \boldsymbol{Q}$, respectively. The polarizability of any of the modes is given by Eq. (29), while the Green's function for the electric field can be recast as [cf. Eq. (32b)]

$$D_L^E(\Omega,\boldsymbol{Q}) = -2\pi\sqrt{Q^2 - (\Omega/c)^2 - i0}, \tag{D1a}$$

$$D_T^E(\Omega,\boldsymbol{Q}) = \frac{2\pi(\Omega/c)^2}{\sqrt{Q^2 - (\Omega/c)^2 - i0}}. \tag{D1b}$$

The dispersion of excitons with allowance for the light-matter interaction can be found from the self-consistency requirement with the result:

$$\pi_1(\Omega,\boldsymbol{Q})D_{L,T}^E(\Omega,\boldsymbol{Q}) = 1. \tag{D2}$$

At $\boldsymbol{Q} = 0$, we obtain the radiative damping of the excitons in the form

$$\hbar\Gamma_0 = 2\pi\frac{E_g - E_B}{\hbar c}d_{\rm exc}^2. \tag{D3}$$

The exciton LT splitting [at $Q \gg (E_g - E_B)/\hbar c$, i.e., where the retardation is not important] is

$$\Delta E_{\rm LT} = 2\pi Q d_{\rm exc}^2 = \frac{\hbar c Q}{E_g - E_B}\hbar\Gamma_0, \tag{D4}$$

in full agreement with previous works.

Interestingly, for noncondensed excitons with $E_B = E_g$ (just at the threshold of exciton insulator instability), the dispersion of the longitudinal and transverse branches as $Q \to 0$ is given by

$$E_L^0(Q) = \frac{d_{\rm exc}^2 Q}{1 + \frac{d_{\rm exc}^4}{\hbar^2 c^2}} \approx \begin{cases} d_{\rm exc}^2 Q, & d_{\rm exc}^2 \ll \hbar c, \\ \frac{\hbar^2 c^2}{d_{\rm exc}^4}Q, & d_{\rm exc}^2 \gg \hbar c. \end{cases} \tag{D5a}$$

$$E_T^0(Q) = \frac{\hbar^2 Q^2}{2M} - 2\pi d_{\rm exc}^2\frac{\hbar^2 Q^3}{(2Mc)^2}. \tag{D5b}$$

While the transversal branch remains parabolic with small correction $\propto Q^3$, the longitudinal branch acquires a linear dispersion. Its propagation velocity is always smaller that c because of the causuality imposed by the light-matter interaction.

APPENDIX E: EVALUATION OF $N_{\rm exc}$

According to Eq. (40), we have in the limit of very low temperatures where the small-Q, small-φ asymptotics is valid

$$N_{\rm exc} = \frac{k_B T}{2(2\pi)^3 d_{\rm exc}^2}\int\frac{Q^2 dQ d\varphi}{Q^2\varphi^2 + (\xi/c)^2 Q^3}, \tag{E1}$$

where the limits of the integral should be chosen in such a way that $\mathcal{E}(\boldsymbol{Q}) \lesssim k_B T$. Using the interpolation expression for

the energy (35), we obtain $|\varphi| < \varphi_Q \equiv k_B T/(\hbar c Q)$ and the angular integral is evaluated as

$$\int_{-\varphi_Q}^{\varphi_Q} d\varphi \frac{Q^2}{Q^2\varphi^2 + (\xi/c)^2 Q^3} = \frac{2c}{\sqrt{Q}\xi} \tan^{-1}\left(\frac{k_B T}{\hbar \xi Q^{3/2}}\right).$$

The remaining integral over Q can now be easily calculated, giving the result

$$N_{\rm exc} = \frac{k_B T}{2(2\pi)^3 d_{\rm exc}^2} \times \frac{4\pi c}{\sqrt{3}} \left(\frac{k_B T}{\hbar \xi^4}\right)^{1/3}, \tag{E2}$$

in agreement with Eq. (42).

[1] L. V. Keldysh and Y. V. Kopaev, Possible instability of semimetallic state toward Coulomb interaction, Phys. Solid State **6**, 2219 (1965).

[2] D. Jérome, T. M. Rice, and W. Kohn, Excitonic insulator, Phys. Rev. **158**, 462 (1967).

[3] H. Cercellier, C. Monney, F. Clerc, C. Battaglia, L. Despont, M. G. Garnier, H. Beck, P. Aebi, L. Patthey, H. Berger, and L. Forró, Evidence for an excitonic insulator phase in $1T$–$TiSe_2$, Phys. Rev. Lett. **99**, 146403 (2007).

[4] K. Seki, Y. Wakisaka, T. Kaneko, T. Toriyama, T. Konishi, T. Sudayama, N. L. Saini, M. Arita, H. Namatame, M. Taniguchi, N. Katayama, M. Nohara, H. Takagi, T. Mizokawa, and Y. Ohta, Excitonic Bose-Einstein condensation in Ta_2NiSe_5 above room temperature, Phys. Rev. B **90**, 155116 (2014).

[5] L. Du, X. Li, W. Lou, G. Sullivan, K. Chang, J. Kono, and R.-R. Du, Evidence for a topological excitonic insulator in InAs/GaSb bilayers, Nat. Commun. **8**, 1971 (2017).

[6] A. Kogar, M. S. Rak, S. Vig, A. A. Husain, F. Flicker, Y. I. Joe, L. Venema, G. J. MacDougall, T. C. Chiang, E. Fradkin, J. van Wezel, and P. Abbamonte, Signatures of exciton condensation in a transition metal dichalcogenide, Science **358**, 1314 (2017).

[7] S. S. Ataei, D. Varsano, E. Molinari, and M. Rontani, Evidence of ideal excitonic insulator in bulk MoS_2 under pressure, Proc. Natl. Acad. Sci. USA **118**, e2010110118 (2021).

[8] Z. Sun, Y. Murakami, F. Xuan, T. Kaneko, D. Golež, and A. J. Millis, Dynamical exciton condensates in biased electron-hole bilayers, Phys. Rev. Lett. **133**, 217002 (2024).

[9] L. Ma, P. X. Nguyen, Z. Wang, Y. Zeng, K. Watanabe, T. Taniguchi, A. H. MacDonald, K. F. Mak, and J. Shan, Strongly correlated excitonic insulator in atomic double layers, Nature (London) **598**, 585 (2021).

[10] N. D. Mermin and H. Wagner, Absence of ferromagnetism or antiferromagnetism in one- or two-dimensional isotropic Heisenberg models, Phys. Rev. Lett. **17**, 1133 (1966).

[11] P. C. Hohenberg, Existence of long-range order in one and two dimensions, Phys. Rev. **158**, 383 (1967).

[12] L. C. Andreani and F. Bassani, Exchange interaction and polariton effects in quantum-well excitons, Phys. Rev. B **41**, 7536 (1990).

[13] M. M. Glazov, T. Amand, X. Marie, D. Lagarde, L. Bouet, and B. Urbaszek, Exciton fine structure and spin decoherence in monolayers of transition metal dichalcogenides, Phys. Rev. B **89**, 201302(R) (2014).

[14] H. Yu, G.-B. Liu, P. Gong, X. Xu, and W. Yao, Dirac cones and Dirac saddle points of bright excitons in monolayer transition metal dichalcogenides, Nat. Commun. **5**, 3876 (2014).

[15] D. Y. Qiu, T. Cao, and S. G. Louie, Nonanalyticity, valley quantum phases, and lightlike exciton dispersion in monolayer transition metal dichalcogenides: Theory and first-principles calculations, Phys. Rev. Lett. **115**, 176801 (2015).

[16] V. M. Agranovich and M. D. Galanin, *Electronic Excitation Energy Transfer in Condensed Matter* (North-Holland Publishing Company, Amsterdam, 1982).

[17] A. M. Shentsev and M. M. Glazov, Electromagnetic field assisted exciton diffusion in moiré superlattices, Phys. Rev. B **111**, 045301 (2025).

[18] T. Portengen, Th. Östreich, and L. J. Sham, Theory of electronic ferroelectricity, Phys. Rev. B **54**, 17452 (1996).

[19] Z. Sun, T. Kaneko, D. Golež, and A. J. Millis, Second-order Josephson effect in excitonic insulators, Phys. Rev. Lett. **127**, 127702 (2021).

[20] P. I. Arseev, Electrostatic mechanism of ferroelectric instability, Fiz. Tverd. Tela **67**, 314 (2025).

[21] H. Yu, G.-B. Liu, and W. Yao, Brightened spin-triplet interlayer excitons and optical selection rules in van der Waals heterobilayers, 2D Mater. **5**, 035021 (2018).

[22] M. Förg, L. Colombier, R. K. Patel, J. Lindlau, A. D. Mohite, H. Yamaguchi, M. M. Glazov, D. Hunger, and A. Högele, Cavity-control of interlayer excitons in van der Waals heterostructures, Nat. Commun. **10**, 3697 (2019).

[23] K. K. Grigoryan and M. M. Glazov, Intersubband electric dipole spin resonance in transition metal dichalcogenide heterobilayers, Phys. Rev. B **113**, 179605 (2026).

[24] M. A. Semina, Excitons and trions in bilayer van der Waals heterostructures, Phys. Solid State **61**, 2218 (2019).

[25] V. V. Tolmachev and S. V. Tiablikov, A new method in the theory of superconductivity. II, J. Exptl. Theoret. Phys. (U.S.S.R.) **34**, 66 (1958) [JETP **34**, 46 (1958)].

[26] A. N. Kozlov and L. A. Maksimov, The metal-dielectric divalent crystal phase transition, J. Exptl. Theoret. Phys. (U.S.S.R.) **48**, 1184 (1965) [JETP **21**, 790 (1965)].

[27] A. N. Kozlov and L. A. Maksimov, Collective excitations in semimetals, J. Exptl. Theoret. Phys. (U.S.S.R.) **49**, 1284 (1965) [JETP **22**, 889 (1966)].

[28] R. R. Guseinov and L. V. Keldysh, Nature of the phase transition under the conditions of an "excitonic" instability in the electronic spectrum of a crystal, Zh. Eksp. Teor. Fiz. **63**, 2255 (1972) [JETP **36**, 1193 (1973)].

[29] Yu. E. Lozovik and V. I. Yudson, A new mechanism for superconductivity: Pairing between spatially separated electrons and holes, Zh. Eksp. Teor. Fiz. **71**, 738 (1976) [JETP **44**, 389 (1976)].

[30] Yu. E. Lozovik and V. I. Yudson, The phase fixation in the systems with e-h pairing; collective modes and current states, Solid State Commun. **22**, 117 (1977).

[31] P. B. Littlewood, P. R. Eastham, J. M. J. Keeling, F. M. Marchetti, B. D. Simons, and M. H. Szymanska, Models of coherent exciton condensation, J. Phys.: Condens. Matter **16**, S3597 (2004).

[32] E. Manousakis, Transition to an excitonic insulator from a two-dimensional conventional insulator, Phys. Rev. B **107**, 075105 (2023).

[33] M. Trushin, Interlayer excitonic insulator in two-dimensional double-layer semiconductor junctions: An explicitly solvable model, Phys. Rev. B **106**, 125311 (2022).

[34] V. L. Berezinskii, Destruction of long-range order in one-dimensional and two-dimensional systems having a continuous symmetry group I. Classical systems, Zh. Eksp. Teor. Fiz. **59**, 907 (1970) [JETP **32**, 493 (1971)].

[35] V. L. Berezinskii, Destruction of long-range order in one-dimensional and two-dimensional systems possessing a continuous symmetry group. II. Quantum systems, Zh. Eksp. Teor. Fiz. **61**, 1144 (1971) [JETP **34**, 610 (1972)].

[36] J. M. Kosterlitz and D. J. Thouless, Ordering, metastability and phase transitions in two-dimensional systems, J. Phys. C: Solid State Phys. **6**, 1181 (1973).

[37] E. M. Lifshitz and L. P. Pitaevskii, *Statistical Physics: Theory of the Condensed State* (Butterworth-Heinemann, Oxford, 2002).

[38] E. L. Ivchenko, *Optical Spectroscopy of Semiconductor Nanostructures* (Alpha Science, Harrow, UK, 2005).

[39] F. Stern, Polarizability of a two-dimensional electron gas, Phys. Rev. Lett. **18**, 546 (1967).

[40] A. V. Chaplik, Absorption and emission of electromagnetic waves by two-dimensional plasmons, Surf. Sci. Rep. **5**, 289 (1985).

[41] M. Z. Maialle, E. A. de A. e. Silva, and L. J. Sham, Exciton spin dynamics in quantum wells, Phys. Rev. B **47**, 15776 (1993).

[42] S. V. Gupalov, E. L. Ivchenko, and A. V. Kavokin, Fine structure of localized exciton levels in quantum wells, J. Exp. Theor. Phys. **86**, 388 (1998).

[43] P. W. Anderson, Random-phase approximation in the theory of superconductivity, Phys. Rev. **112**, 1900 (1958).

[44] P. B. Littlewood and C. M. Varma, Amplitude collective modes in superconductors and their coupling to charge-density waves, Phys. Rev. B **26**, 4883 (1982).

[45] D. Pekker and C. M. Varma, Amplitude/Higgs modes in condensed matter physics, Annu. Rev. Condens. Matter Phys. **6**, 269 (2015).

[46] P. W. Anderson, Higgs, Anderson and all that, Nat. Phys. **11**, 93 (2015).

[47] A. Altland and B. D. Simons, *Condensed Matter Field Theory*, 2nd ed. (Cambridge University Press, Cambridge, 2010).

[48] W. Chen, C.-J. Huang, and Q. Zhu, Searching for unconventional superfluid in excitons of monolayer semiconductors, Phys. Rev. Lett. **131**, 236004 (2023).

[49] A. Griffin, D. W. Snoke, and S. Stringari, *Bose-Einstein Condensation* (Cambridge University Press, Cambridge, 1996).

[50] K. Huang, C. N. Yang, and J. M. Luttinger, Imperfect Bose gas with hard-sphere interaction, Phys. Rev. **105**, 776 (1957).

[51] P. E. Faria, Jr. and J. Fabian, Signatures of electric field and layer separation effects on the spin-valley physics of $MoSe_2/WSe_2$ heterobilayers: From energy bands to dipolar excitons, Nanomaterials **13**, 1187 (2023).

[52] R. Gillen, Interlayer excitonic spectra of vertically stacked $MoSe_2/WSe_2$ heterobilayers, Phys. Status Solidi (B) **258**, 2000614 (2021).

[53] L. P. Pitaevskii and S. Stringari, *Bose-Einstein Condensation*, International Series of Monographs on Physics (Clarendon Press, Oxford, 2003).

[54] M. M. Glazov and R. A. Suris, Collective states of excitons in semiconductors, Phys. Usp. **63**, 1051 (2021).

[55] C. Poellmann, P. Steinleitner, U. Leierseder, P. Nagler, G. Plechinger, M. Porer, R. Bratschitsch, C. Schuller, T. Korn, and R. Huber, Resonant internal quantum transitions and femtosecond radiative decay of excitons in monolayer WSe_2, Nat. Mater. **14**, 889 (2015).

[56] A. Kormanyos, G. Burkard, M. Gmitra, J. Fabian, V. Zólyomi, N. D Drummond, and V. Fal'ko, $\mathbf{k}\cdot\mathbf{p}$ theory for two-dimensional transition metal dichalcogenide semiconductors, 2D Mater. **2**, 022001 (2015).

[57] M. M. Glazov, L. E. Golub, G. Wang, X. Marie, T. Amand, and B. Urbaszek, Intrinsic exciton-state mixing and nonlinear optical properties in transition metal dichalcogenide monolayers, Phys. Rev. B **95**, 035311 (2017).

[58] K.-Q. Lin, C. S. Ong, S. Bange, P. E. Faria, Jr., B. Peng, J. D. Ziegler, J. Zipfel, C. Bäuml, N. Paradiso, K. Watanabe, T. Taniguchi, C. Strunk, B. Monserrat, J. Fabian, A. Chernikov, D. Y. Qiu, S. G. Louie, and J. M. Lupton, Narrow-band high-lying excitons with negative-mass electrons in monolayer WSe_2, Nat. Commun. **12**, 5500 (2021).

[59] K.-Q. Lin, J. D. Ziegler, M. A. Semina, J. V. Mamedov, K. Watanabe, T. Taniguchi, S. Bange, A. Chernikov, M. M. Glazov, and J. M. Lupton, High-lying valley-polarized trions in 2D semiconductors, Nat. Commun. **13**, 6980 (2022).

[60] K.-Q. Lin, P. E. Faria, Jr., R. Hübner, J. D. Ziegler, J. M. Bauer, F. Buchner, M. Florian, F. Hofmann, K. Watanabe, T. Taniguchi, J. Fabian, A. Steinhoff, A. Chernikov, S. Bange, and J. M. Lupton, Ultraviolet interlayer excitons in bilayer WSe_2, Nat. Nanotechnol. **19**, 196 (2024).

[61] I. Amelio, N. D. Drummond, E. Demler, R. Schmidt, and A. Imamoglu, Polaron spectroscopy of a bilayer excitonic insulator, Phys. Rev. B **107**, 155303 (2023).

[62] Y. Xu, S. Liu, D. A. Rhodes, K. Watanabe, T. Taniguchi, J. Hone, V. Elser, K. F. Mak, and J. Shan, Correlated insulating states at fractional fillings of moiré superlattices, Nature (London) **587**, 214 (2020).

[63] C. Zerba, C. Kuhlenkamp, A. Imamoglu, and M. Knap, Realizing topological superconductivity in tunable Bose-Fermi mixtures with transition metal dichalcogenide heterostructures, Phys. Rev. Lett. **133**, 056902 (2024).

[64] J. von Milczewski, X. Chen, A. Imamoglu, and R. Schmidt, Superconductivity induced by strong electron-exciton coupling in doped atomically thin semiconductor heterostructures, Phys. Rev. Lett. **133**, 226903 (2024).

[65] M. Xie, M. Hafezi, and S. Das Sarma, Long-lived topological flatband excitons in semiconductor moiré heterostructures:

A bosonic Kane-Mele model platform, Phys. Rev. Lett. **133**, 136403 (2024).

[66] R. Perea-Causin, H. Liu, and E. J. Bergholtz, Exciton fractional Chern insulators in moiré heterostructures, Phys. Rev. Res. **7**, L042033 (2025).

[67] Y. Ashida, A. Imamoglu, J. Faist, D. Jaksch, A. Cavalleri, and E. Demler, Quantum electrodynamic control of matter: Cavity-enhanced ferroelectric phase transition, Phys. Rev. X **10**, 041027 (2020).

[68] H. Gao, F. Schlawin, and D. Jaksch, Higgs mode stabilization by photoinduced long-range interactions in a superconductor, Phys. Rev. B **104**, L140503 (2021).

[69] L. V. Keldysh and A. N. Kozlov, Collective properties of excitons in semiconductors, Sov. Phys. JETP **27**, 79 (1968).